



Scatter

User Manual

Created by Stefano Galvan, Stewart Haslinger, Fan Shi,
Peter Huthwaite, Richard Craster and Mike Lowe.

Scatter belongs to Imperial College London.

For information, please contact Mike Lowe at info@scatter.software.

This version of the user manual is provided for the software release of
the same version number.

Scatter version 1.0.0

November 2021

Contents

1	Introduction	2
1.1	Software requirements	2
1.2	Conditions of release	2
1.2.1	Compliance with LGPL	2
1.2.2	Written offer to provide 3rd-party source code	4
2	Getting started quickly with Scatter	4
2.1	Input/Output tab	5
2.2	Case study	6
2.2.1	Materials	6
2.2.2	Type of incident wave	7
2.2.3	Surface	7
2.2.4	Signal	14
2.2.5	Source	14
2.2.6	Receivers	19
2.2.7	Calculation	21
2.3	Outputs	22
2.4	Exporting output files	27
3	Underlying theory	27
3.1	Rough surfaces	27
3.2	Kirchhoff Approximation	29
3.2.1	Reflection coefficients	31
3.3	Formulation of scattering problem	32
4	Tutorial case studies	34
4.1	Defect 1 (no tilt)	35
4.2	Defect 2 (tilted in anticlockwise direction)	39
4.3	Defect 3 (tilted in clockwise direction)	41
	Bibliography	45

1 Introduction

Scatter is a software package designed to rapidly calculate ultrasonic scattering amplitudes and intensities using analytical and theoretical modelling methods. Version 1.0.0 has capability for calculating reflection amplitudes for finite planar rough defects in two-dimensional space. Outputs are normalised with respect to amplitudes computed for smooth defects of the same size. The predicted amplitudes are evaluated using Kirchhoff Approximation (KA) scattering integrals, which are implemented for a variety of excitations, source and receiver set-ups and material parameters. All elastic wave mode conversions are taken into account.

1.1 Software requirements

Scatter is available for MS Windows, macOS and Linux. Scatter has been tested and it is known to work in

- Windows 10+
- macOS 10.12+
- Ubuntu 16.04+ or other equivalent distributions.

Please note that Scatter has not been developed for the new Apple Silicon, e.g. M1, architecture. It may work but it has not been tested.

There are no specific hardware requirements, any modern computer should be able to run Scatter. Scatter uses OpenGL and may not work on virtual machines. Scatter is not suitable for remote execution.

1.2 Conditions of release

Scatter and libScatterCore belong to Imperial College. They may not be re-distributed. By using the software, users agree that it is provided without warranty of any kind, and agree not to hold Imperial College or the software developers responsible for any damages that might arise from the results, including any errors in the researched algorithms or the implementations in coding.

1.2.1 Compliance with LGPL

Scatter uses the Qt framework under the terms of LGPL. Scatter complies with LGPL in the following ways:

- Scatter dynamically links to the unmodified Qt libraries.
- All users of Scatter are expressly allowed to change and re-link their own versions of the Qt libraries, as long as they remain interface-compatible with the libraries originally used to build Scatter. User-selected Qt libraries can be re-linked using appropriate tools of the operating system, such as

`LD_LIBRARY_PRELOAD` (Linux)

and

`DYLD_INSERT_LIBRARIES` (macOS)

or similar. The easiest solution is to overwrite the libraries provided with Scatter with the custom ones. In details:

Windows Qt libraries are stored inside the main directory, together with the `Scatter.exe` executable.

macOS Qt libraries are stored inside the Scatter bundle (usually installed in `Applications`), in the directory `Contents→Frameworks`.

The names of the libraries, and their precise locations, are:

- `QtWidgets` in `QtWidgets.framework→Versions→5`
- `QtSql` in `QtSql.framework→Versions→5`
- `QtPrintSupport`
in `QtPrintSupport.framework→Versions→5`
- `QtOpenGL` in `QtOpenGL.framework→Versions→5`
- `QtGui` in `QtGui.framework→Versions→5`
- `QtDBus` in `QtDBus.framework→Versions→5`
- `QtCore` in `QtCore.framework→Versions→5`

Linux Qt libraries are stored inside the main directory, together with the `Scatter` executable and the `Scatter.sh` starting script.

- Every installation of Scatter contains the copy of the applicable Qt licenses. They are stored differently depending on the operating system. In details:

Windows Licenses are stored inside the main directory, together with the `Scatter.exe` executable.

macOS Licenses are stored inside the Scatter bundle (usually installed in `Applications`), in the directory `Contents→Resources`. To get access to the bundle it is enough to right-click on the Scatter app icon and select “Show Package Contents”.

Linux Licenses are stored inside the main directory, together with the Scatter executable and the `Scatter.sh` starting script.

- The Info dialog box of Scatter prominently states that this program uses the Qt libraries under the terms of LGPL, including the exact version and any copyright information.

1.2.2 Written offer to provide 3rd-party source code

As a Scatter user, you may obtain a copy of the source code for Qt (same version provided with the installation of Scatter) by sending a written request to: `info@scatter.software`. Please indicate which specific version of Scatter you are using. Each Qt version will be available for a period of three (3) years from the date of release or date of purchase, whichever expires later.

2 Getting started quickly with Scatter

Scatter may be used to generate both smooth and rough planar defects in two-dimensional (2-D) space. The setup consists of a continuous expanse of material in the XY -plane, within which the user can define a defect of specified size, orientation and roughness. The rough crack has its centre at $X = 0$ and the tilt angle is measured relative to the line $Y = 0$, in the anticlockwise direction. Three choices of excitation are available to generate incident waves, which initiate from somewhere in the positive half-plane (i.e. positive Y location), travelling downwards towards the crack. Scatter calculates the amplitudes of the waves scattered back from the defect, measured relative to the scattered amplitude for a smooth crack, of the same size and for normally incident waves generated by the same excitation method.

The software package comes with a pre-loaded case study which is described in detail here to summarise how to use Scatter and to demonstrate its flexibility and capabilities. New users are encouraged to work through this case study and the explanations related to the pre-loaded example values in order to become familiar with the working processes for the software package, as well as its key menus and features. Additional case study examples, and the corresponding datasets in CSV (comma-separated value) format, are also provided at the end of this manual. Explanations throughout the case study and tutorial examples show where the user may make different choices for new cases of interest.

Note that to start Scatter using a Linux OS, it is necessary to run <code>Scatter.sh</code> .

2.1 Input/Output tab

After opening Scatter, the user is presented with a graphical window showing a finite rough surface (blue), a schematic representation of an incident plane wave (green) and an array of receivers (red points). All three of these pre-loaded selections may be altered using the categories within the Input tab, which is one of two options (along with Output) in the top left of the screen. Toggling between the two allows the user to see the pre-loaded reflection amplitude results for the case study. The user is also able to access this manual directly from Scatter by clicking on the Info tab in the top left corner.

In the initial graphical window, the user will also observe that dimensions are provided in millimetres, which reflects the fact that the package is designed for applications in ultrasonic non-destructive evaluation (NDE), for which typical wavelengths and length scales are measured in millimetres. For example, the wavelength of a compression (P-) wave, with centre frequency 5MHz, that propagates in a stainless steel sample is around 1.2mm. It should also be noted that the user may focus on specific areas of the graphical window, by clicking the left button on one's mouse and scrolling to adjust the centre of the window frame, and then scrolling with the mouse wheel to zoom in or out. The capability to zoom into a specific region is possible for both input or output panels, and at any time.

The input tab is used for the problem description and model generation. It is divided into six categories to input the following model settings:

- Material parameters;
- Type of incident wave;
- Rough surface;
- Signal;
- Source excitation;
- Receivers.

The final sub-category is Calculation and this enables the user to select the type of scattering theory to implement for the calculation of the reflection amplitudes for the problem defined by the preceding user-defined model settings. In version 1.0.0, only the Kirchhoff Approximation model is available but subsequent software updates will incorporate alternative modelling approaches.

Each sub-category has an `Apply` button, which must be used to update any parameter settings. The Calculation tab has a `Compute` button in place

of `Apply`, and this should only be used after all applications of `Apply` have been completed, checked and finalised.

2.2 Case study

The problem formulation for the pre-loaded case study is explained in detail, with each model-setting category addressed in descending order. The case study example is a planar rough surface of length 8mm, characterised by two roughness parameter values. As explained in detail in Section 3.1, statistical probability distributions can be used to characterise rough surfaces. Although specific statistical roughness parameter definitions may differ slightly, it is important to quantify the variation of height above and below a mean reference line/plane and the lateral variation along the length of the rough surface. Scatter uses the rms height σ and the correlation length λ_0 , both defined by Gaussian distributions, to characterise the rough surfaces generated. The case study example was generated for $\sigma = 0.15\text{mm}$ and $\lambda_0 = 0.6\text{mm}$.

The rough surface is always centred at the origin in Scatter, both those generated by Scatter and imported. In the case study explanations that follow, an array of Source and Receiver set-ups are described, enabling the user to familiarise oneself with the features and capabilities available for addressing new cases. Three additional datasets are provided, which can be imported for use within the tutorials described in Section 4.

2.2.1 Materials

The first choice for the user to make is the material in which the rough surface/defect is embedded. In version 1.0.0, the user must input their own specific material parameters (future versions may include common predefined materials) and there are two ways to do this, with identical results. After clicking on the Materials tab, the pre-selected option of Speeds is opened. As can be seen in Figure 1a, bulk wave speeds for compression c_1 (P- or longitudinal) and shear c_s (S- or transverse) waves are entered (up to two decimal places) along with material density ρ (rho). Standard SI units of m/s and kg/m³ are used.

The alternative method for inputting the required material parameters is accessible via the Elastic tab (see the bottom of either Figure 1a or 1b), which also reveals three values to be entered, as shown in Figure 1b. This option allows the user to input Young's modulus E and Poisson ratio ν (nu) values together with the material density, from which the elastic bulk wave speeds are calculated. Note that the two methods are interconnected and that varying the parameters under either the Speeds or Elastic tab will

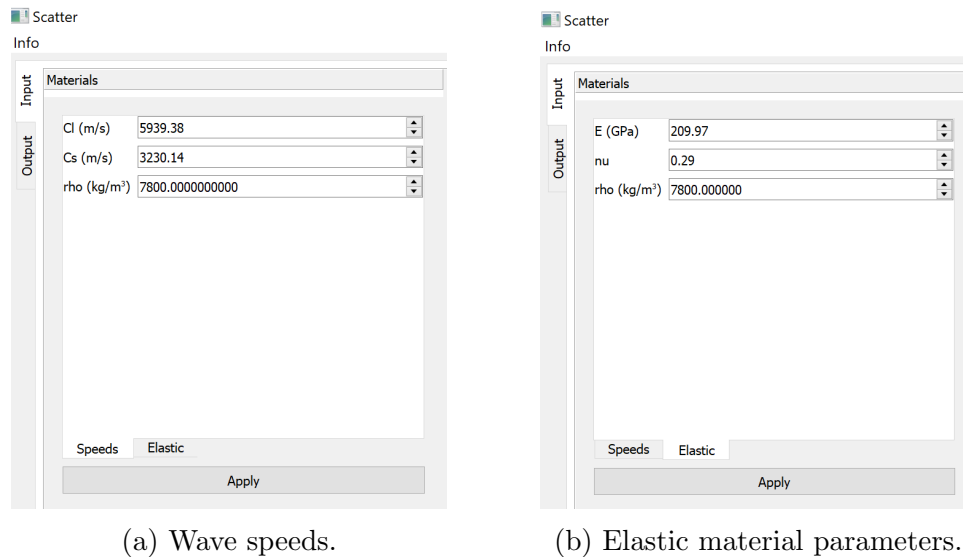


Figure 1: Two options under Materials tab for selecting underlying material parameters.

simultaneously alter the values under the other tab. The units for Young's modulus are GPa, and the Poisson ratio is dimensionless. Once the user has entered the desired material parameter values, in order to update the model, the `Apply` button must be clicked. Without pressing `Apply`, the pre-loaded (or previously used) values will be retained. The case study uses stainless steel material parameters.

2.2.2 Type of incident wave

Scatter is an elastic wave-based modelling tool and therefore any problem includes compression and shear waves. The Input sub-category Incident Wave enables the user to select either a compression or shear incident wave type. As for all Input sections, the choice is finalised after pressing the `Apply` button.

2.2.3 Surface

This sub-category is considerably more involved than the previous two. The primary function is to either generate or import the finite rough surface/defect under investigation. More details on randomly rough defects and methods for modelling them are included in Section 3.1 but here information is restricted to use of the software, with reference to the case study. The Surface

tab is shown in Figure 2, and below the numerical input boxes, there are two options of Generate and Load Surface.

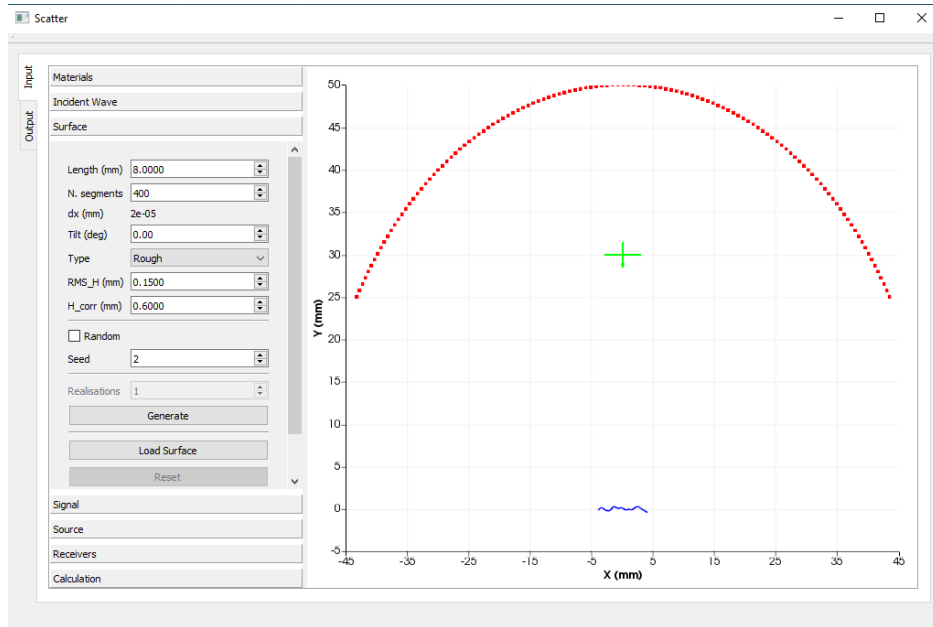


Figure 2: Generating or loading a finite rough surface.

The user may choose to import a specific rough (or smooth) surface of interest by clicking on the `Load Surface` button, which then requests CSV (comma-separated value) format. Upon loading the surface, the schematic illustration of the surface automatically changes, as illustrated in Figure 3 which shows a different surface to the pre-loaded case study surface in Figure 2. The other notable feature of selecting the `Load Surface` option is that the rest of the `Surface` box is then disabled (the input boxes in Figure 3 are greyed out). This means that the user, in loading surface data, has predefined the roughness, length, discretisation and tilt of the surface and so Scatter does not require this information to proceed with the model description. These inputs are required by Scatter to generate a surface but version 1.0.0 does not evaluate the roughness statistical parameter values from a surface that has been loaded. In future releases, this feature may be enabled. Also, only CSV format is supported at the time of writing. More information is provided for loading surfaces in the tutorial case studies at the end of the manual.

One of the main features of Scatter is the capability to generate a randomly rough surface and export it. At present, this may be done one at a time, but future releases will support multiple realisations (note the greyed

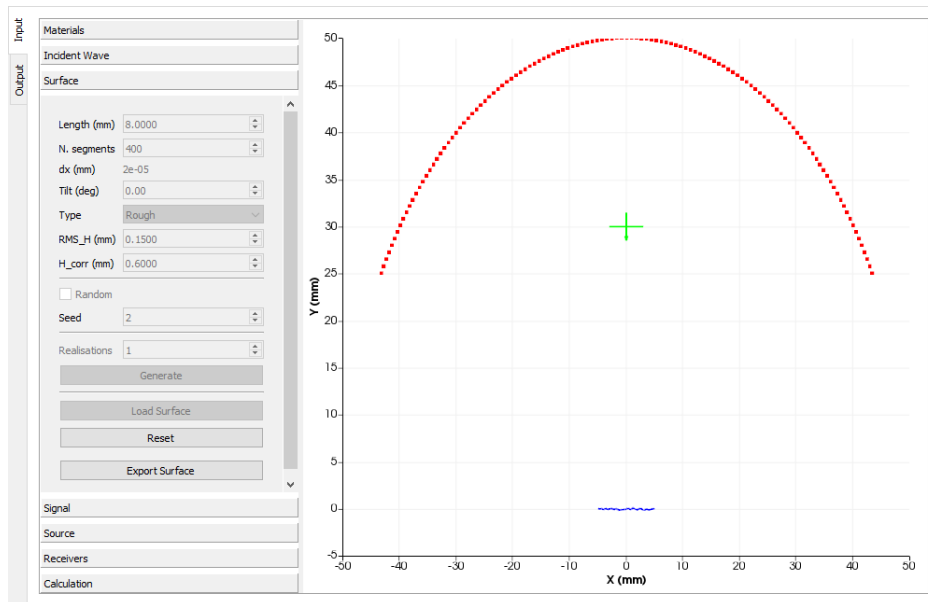


Figure 3: Loading a finite rough surface.

out Realisations input box just above `Generate` in Figure 2). In order to generate a finite rough surface, the following details are required:

- **Length** (in mm);
- **Number of segments** (this determines the discretisation of the surface, the higher this number the better the results for the reflection amplitudes calculated using Kirchhoff Approximation);
- **dx** (mm): this is the discretisation mesh size so the smaller this number the better (it is calculated directly from Length and Number of segments);
- **Tilt angle** ($^{\circ}$): the anticlockwise rotation of a defect, measured in degrees;
- **Type**: the user may choose to generate a finite **smooth** or **rough** defect from a drop-down menu;
- **RMS_H** (in mm), this is the root mean square (rms) height of a rough surface and gives an idea of the variation in height (from $Y = 0$) along the surface;

- **H_corr** (in mm), this is the correlation length of the rough surface and gives an idea of the lateral variation of roughness, i.e. how the peaks and troughs of a rough surface are separated.

Before discussing the embedded random number generator (which is user-controlled), the preceding seven options are expanded upon. Any finite length of surface in millimetres may be chosen, but the software has been extensively tested for defects with length $< 20\text{mm}$ since the primary application of the package is for ultrasonic NDE. An important related factor, which is relevant when selecting the `Source` and `Receiver` settings, is that Kirchhoff approximation is a far field approximation. For larger defects, the receivers should be located further away for better results. The number of segments and discretisation length dx are also directly related to the defect length L and Kirchhoff approximation (KA). As explained in detail in Section 3.2, KA involves computing a numerical integration over the rough surface meaning that the smaller the discretisation length dx (or facet length), the more accurate the evaluation. Therefore, better KA reflection amplitudes results are obtained by increasing the number of segments N , and then dx is calculated according to the equation

$$L = Ndx.$$

The surface generation function also supports tilt of the defect. The user can choose an angle in degrees relative to the line $Y = 0$, resulting in an anticlockwise rotation of the defect about the origin $(X, Y) = (0, 0)$. An example for 10° is shown in Figure 4. Of course, the angle of incidence can also be altered, but this is covered under the `Source` tab. The roughness parameters σ (represented by `RMS_H` in the GUI) and λ_0 (represented by `H_corr`) obey Gaussian roughness distributions (equations are provided in Section 3.1) and chosen values should be entered in millimetres. Reflection amplitudes for rough surfaces using KA rely on the problem being defined for a valid range of roughness for KA to be applicable.

Several research articles have been published with ranges of validity and applicability for Kirchhoff Approximation for rough planar defects and it is recommended to consult them for optimal use of the Gaussian roughness parameters within Scatter. P-wave incidence is covered in detail by [1, 2] and [3] provides comprehensive coverage for S-wave incidence. Some other useful and recent references for typical roughness parameter values for which KA is valid for rough surface reflections are [4–7]. It should be noted that version 1.0.0 has capability for Gaussian roughness distributions and future releases will include additional modelling approaches, such as those described by [8].

Version 1.0.0 also imposes a restriction on correlation lengths (`H_corr`) according to the guidelines published in Table 1 of [7]. Strictly speaking,

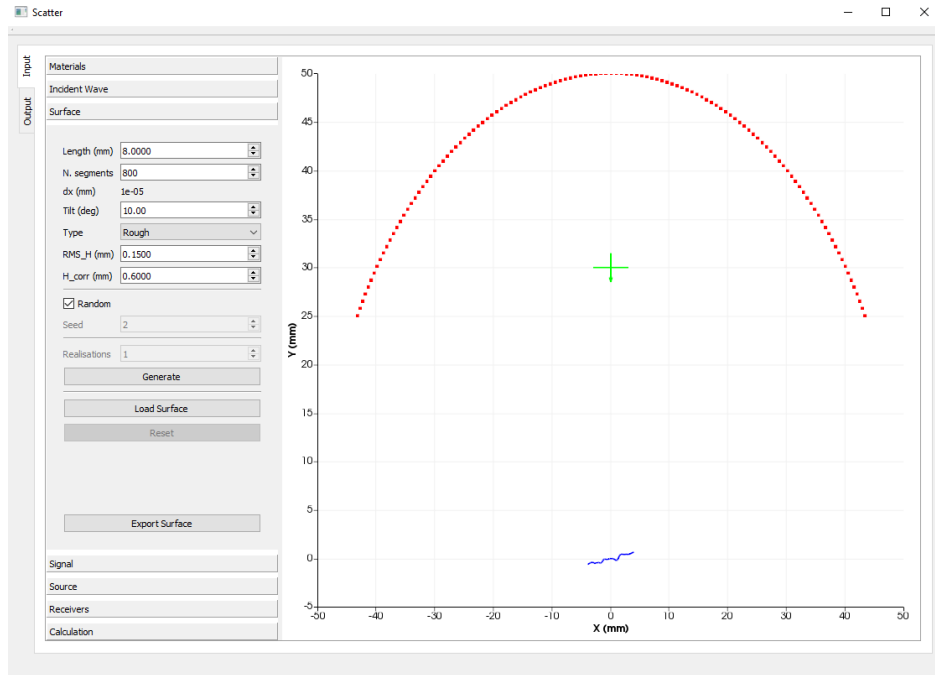


Figure 4: Tilt of a finite rough surface.

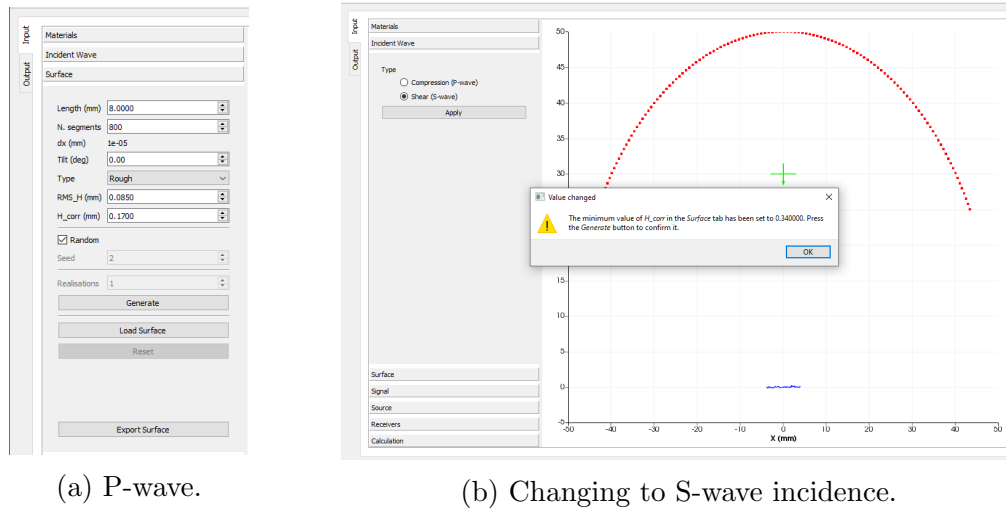
the restriction is dependent on the choice of both rms height and correlation length but since the user selects the rms height σ value first, it is the correlation length λ_0 value that will be automatically shifted to its minimum allowed value given the chosen value of RMS_H and the Incident wave type. This restriction is governed by the two inequalities for P- and S-wave incidence:

$$\begin{aligned} \text{P-wave :} & \quad \frac{\lambda_0}{\sigma} > 1; \\ \text{S-wave :} & \quad \frac{\lambda_0}{\sigma} > 4, \end{aligned}$$

for KA validity.

Let us consider a hypothetical example to illustrate this feature. Assuming P-wave incidence, and roughness values of $\sigma = 0.085\text{mm}$ and $\lambda_0 = 0.17\text{mm}$, Figure 5 shows what the user will see if the wave type incidence is then changed. Since the restriction for RMS_H/H_corr is 0.25, the programme automatically recalibrates the H_corr value to the lowest acceptable value of 0.34mm. Note that the new surface has not been generated at this point. Only once the user presses *Generate*, is this selection confirmed and the corresponding rough surface produced. In the event that a selection of H_corr contravenes the KA validity restriction without changing the Inci-

dent Wave type, the programme automatically restricts H_{corr} but without displaying a warning box.



(a) P-wave.

(b) Changing to S-wave incidence.

Figure 5: Restriction of correlation length value when changing the wave type after defining RMS_H .

The final consideration before confirming the generation of the finite surface is the random number generator. The default seed value, which is a useful feature because it enables the user to generate random numbers that are repeatable, is set to 2. In the event that one forgets to export a particularly interesting surface, rather than never being able to reproduce it, by returning to the same seed value, the surface can be recovered by using the same parameter values for all the preceding options within the Surface tab. To see this process in action, begin from Surface tab for the default case study, shown here in Figure 2.

- Tick the Random option just above seed (the seed box should now be temporarily greyed out);
- Click **Generate** consecutively to produce a random surface each time, similar to that shown in Figure 6;
- Untick the Random box;
- Click **Generate** to reproduce the original case study surface for Seed = 2;
- Now change the Seed to the value 3 and press **Generate** to obtain Figure 7;

- Now change the Seed back to 2 and Generate to recover the original surface again.
- Note that ticking Random from an initial Seed value allows the user to generate randomly rough surfaces characterised by the same parameter values but only the initial surface for a Seed value is always the same.

One final important point to note: in order to generate random surfaces, the Random box must be ticked.

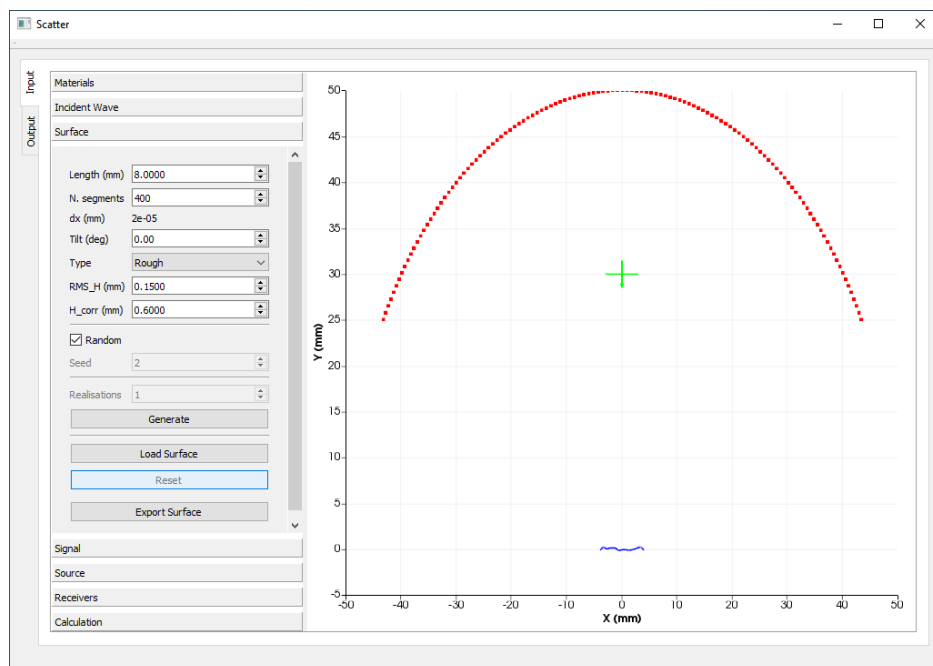


Figure 6: Seed 2, random surface. Note that the Random box is ticked here.

In Figures 6 and 7, the `Reset` option is disabled. This functionality is activated if the option of loading a surface is implemented. In that case, to return to the surface generation mode, click on `Reset` to restore the most recent surface generation settings. Once you have created a rough surface, the dataset can be downloaded by using the `Export Surface` option, from which a comma-separated value (CSV) file can be saved. Three such dataset files have been provided for use with the tutorial examples in Section 4. Note that when exporting a tilted surface, the scattering output results obtained may differ slightly from those obtained when re-importing the same tilted surface at a later date. This is related to the normalisation procedure, which uses a smooth, untilted surface of the same size as the rough surface. This length information is explicit when generating the original surface but when

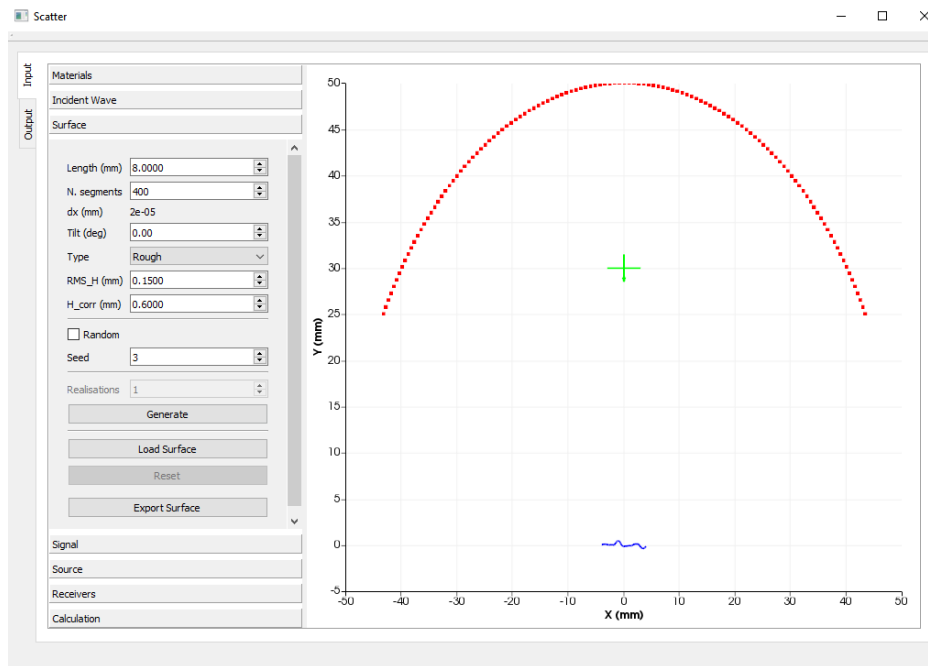


Figure 7: Seed 3, initial surface (different from initial surface for Seed = 2).

importing a CSV file, only the tilted surface height data is available for normalisation. Exported untilted surfaces will produce identical scattering output results to the original computation if re-imported at a later time.

2.2.4 Signal

This allows the user to choose the centre frequency for the investigation, with the units required being MHz. As with Materials and Incident Wave, any changes made must be confirmed by clicking `Apply`.

2.2.5 Source

The `Source` tab enables the user to select one of three excitation types for the source:

- Plane waves;
- Point source;
- Finite transducer.

The default setting in the case study is the first of these, and the direction is determined by the angle (in degrees). Normal incidence, as in the case

study, is defined by 0° . Changing the angle and clicking Apply produces a schematic illustration of the adjusted angle of incidence, as shown in Figure 8. As is clear from this example, the angle is measured anticlockwise with respect to the positive Y -axis.

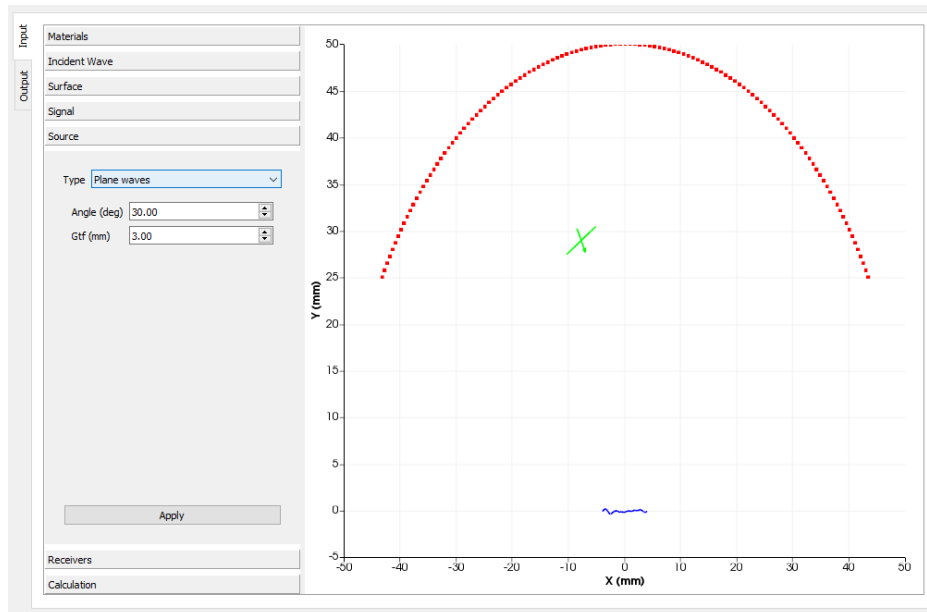


Figure 8: Varying incident angle to 30° .

The other variable within the Plane wave option is the Gaussian tapering function (Gtf) which is an amplitude windowing function that enables the user to reduce the effect of the edges of the finite surface when calculating the KA integral for the scattered field. One of the drawbacks of KA is that it does not account for diffracted waves from the edges of a finite surface/defect. By windowing the plane wave with a Gaussian spatial envelope (Gtf) to impose low amplitudes (compared with unity uniformly across the surface for a pure infinite plane wave) for the exterior parts of the incoming wave (i.e the contributions that will insonify the edges of the defect), one can reduce any inaccuracies that may arise from KA inadequately accounting for these edge effects. In effect, the defect is insonified by a narrower Gaussian beam so that only reflections are included in the integral. Details of this approach are provided by [3, 4] for S- and P-wave incidence, respectively. The value that should be entered is the beam half-width, measured in millimetres such that $2Gtf$ is the approximate length of the surface that is effectively insonified.

For example, if $Gtf = 3\text{mm}$, approximately 6mm of the defect under investigation will be insonified but the outer parts of this 6mm will be insonified

at lower amplitudes than the centre (which will have an amplitude of unity). For the case study's 8mm defect, this setting will produce a different output to an infinite plane wave with no Gtf applied. This is illustrated in Figure 9 where two values are shown, $G_{tf} = 3\text{mm}$ and $G_{tf} = 10\text{mm}$ in Figures 9a and 9b, respectively.

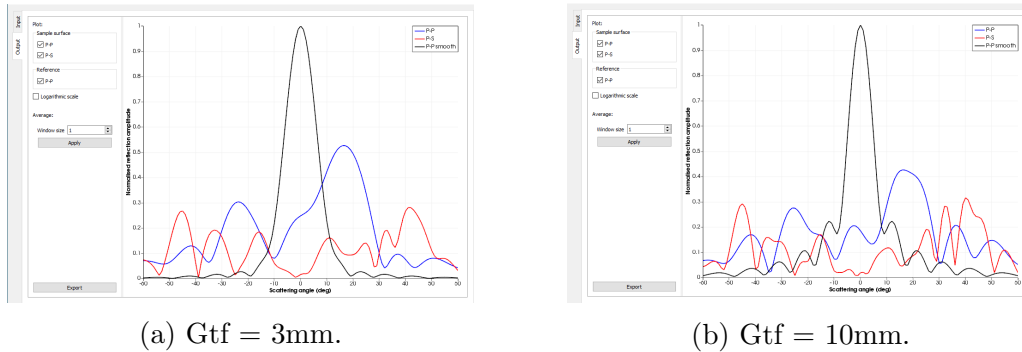


Figure 9: Variation of Gaussian tapering function (G_{tf}) for plane wave incidence.

The outputs are generally covered later on in Section 2.3 but it is instructive to show some results now to explain the use of the G_{tf} feature. Generally, as $G_{tf} \rightarrow \infty$, the windowed incident plane waves tend towards the theoretical infinite plane wave. Therefore, the results for $G_{tf} = 10\text{mm}$ in Figure 9b are effectively the same as if no windowing function was applied since the effective length being insonified is 20mm, which is much greater than the defect length of 8mm. Indeed, if the G_{tf} value is set to 0, no G_{tf} is applied and the same result would be observed. However, the reduced value of $G_{tf} = 3\text{mm}$ shown in Figure 9a is significantly different because less than 6mm of the defect is being insonified with amplitudes equal to unity. The resultant scattered field has larger amplitudes at the central scattering angles than in Figure 9b for this normal incidence case.

The preset value is 5mm and the results for 5mm and no G_{tf} are shown in Figure 10. The results are closer to one another in this case, since an effective 10mm of surface is insonified (which is greater than the length) but due to the Gaussian envelope, the amplitudes decrease away from the centre. However, most of the details are captured by both settings. Notice also the similarity between Figures 9b and 10b and that there is the capability to zoom into regions of the panels, to compare results, by clicking on the left mouse button and scrolling.

The second option for the excitation type is the point source. The required inputs are its location (measured in millimetres relative to the origin)

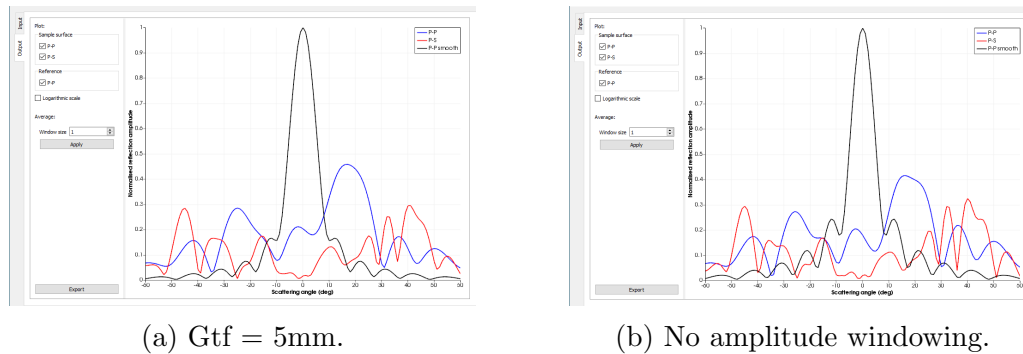


Figure 10: Variation of Gaussian tapering function (Gtf) for plane wave incidence.

so only positive values of Y should be selected, and its amplitude. The further away the point source is located, the closer the results resemble the infinite plane wave case. This is illustrated for the case study in Figure 11, where it is located centrally at a distance of 200mm from the centre of the defect, and the output is similar to the infinite plane wave cases of Figures 9b and 10b. Note that selecting larger incident amplitudes will not result in larger scattered amplitudes in the output, since each case undergoes normalisation to unity (see Section 2.3).

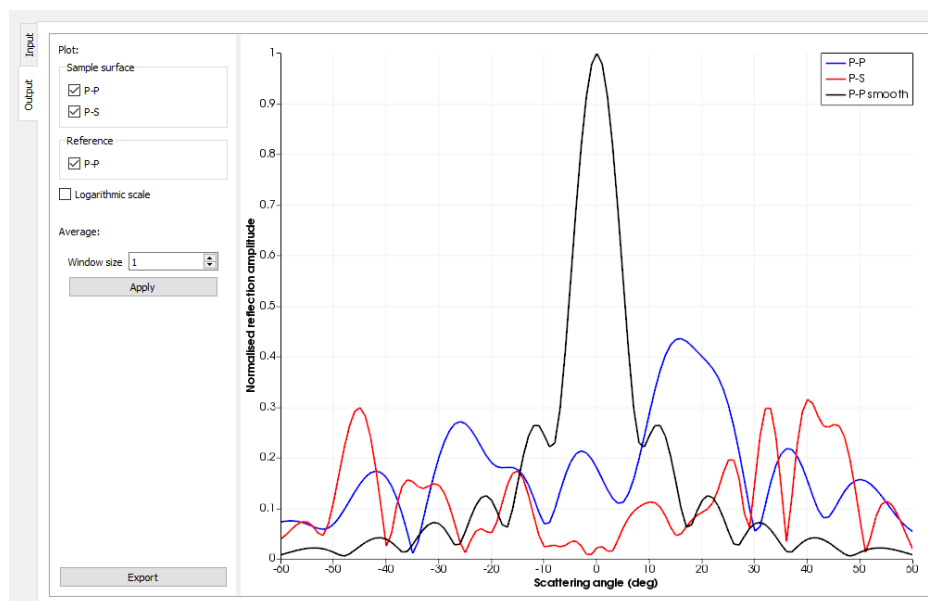


Figure 11: Point source for case study located at (0,200).

A finite transducer option is also available, based on a simple piston

model, which requires the user to enter four characteristic values:

- X -coordinate of the centre of the transducer;
- Y -coordinate of the centre of the transducer (both in millimetres);
- Angle of incidence (in degrees);
- Length of the transducer.

An example for length = 10mm is shown in Figure 12. Note the slightly different schematic representation when compared with the plane wave: two horizontal lines in place of one for the plane wave in Figure 2. A fundamental difference between the finite transducer and the infinite plane wave is that the transducer is discretized into elements over which the fields are averaged. Therefore outputs are likely to be more similar to those arising from the implementation of G_{tf} values for plane waves, rather than pure infinite plane waves, and point sources. It is recommended that the user experiment with the three types of Source available to better understand their similarities and differences.

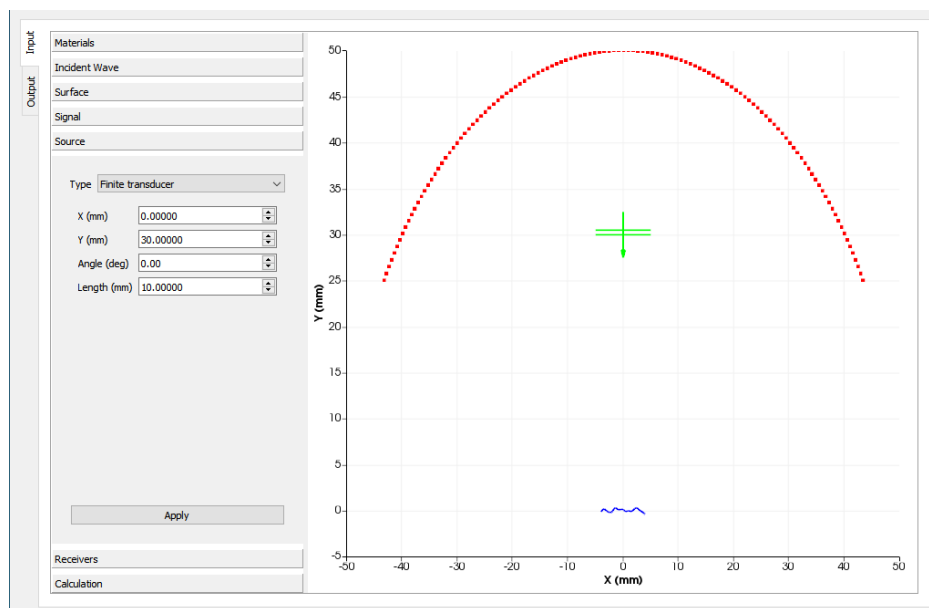


Figure 12: Finite transducer of length 10mm located at (0,30).

2.2.6 Receivers

The final component of the problem description is the Receivers tab which allows the user to select a single receiver or multiple receivers positioned on an arc centred at the origin. The type of receiver is also user-defined, being either a point or a finite transducer (which computes an average over the length of the transducer). The case study setting is for an arc of point receivers, spaced at 1° intervals at a distance of 50mm from the centre of the defect. This is illustrated in Figure 13.

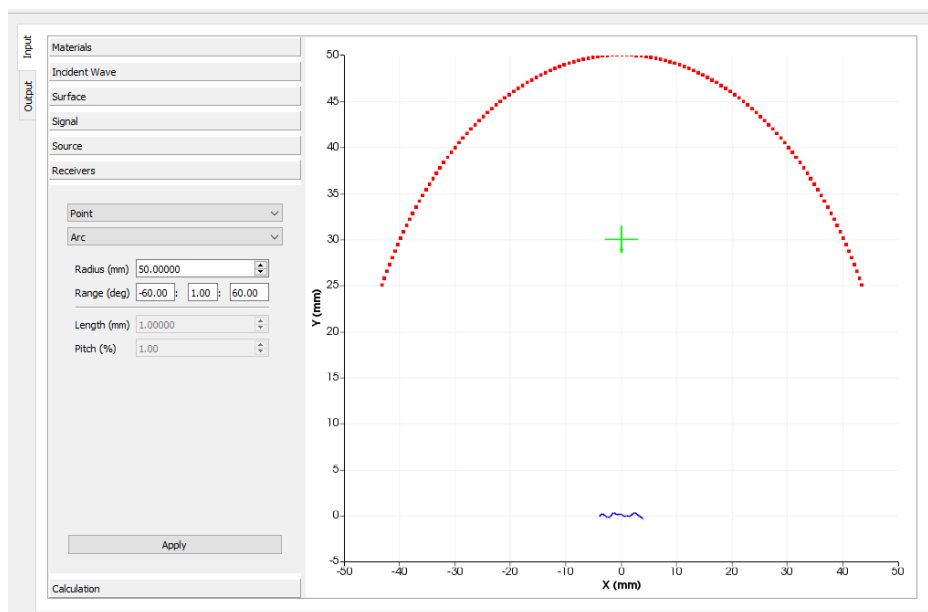


Figure 13: Point receivers located at 50mm and from -60° to 60° at intervals of 1° for the case study example.

There are two drop-down menus within the Receivers tab: Point or Finite Transducer and Arc or Single so that there are four possible combinations presently available:

- Arc of point receivers (default);
- Single point receiver (changing Arc to Single);
- Arc of finite transducers (changing Point to Finite Transducer);
- Single finite transducer (changing both).

The option of Arc enables the user to define its location (by adjusting the radius) and the number of receivers (by adjusting the range in degrees).

The smaller the range discretization (minimum option is 0.5°), the more precise the results. There are two additional inputs disabled in Figure 13, which are enabled if `Point` is switched to `Finite Transducer`, as shown in Figure 14. The choice of finite transducer receivers prompts the user to enter a length in millimetres, and a pitch in % which defines the transducer element size to be the product of this value and the length of the transducer. The reflection amplitude is then averaged over the length of the transducer so that a smaller value of pitch produces a more accurate result.

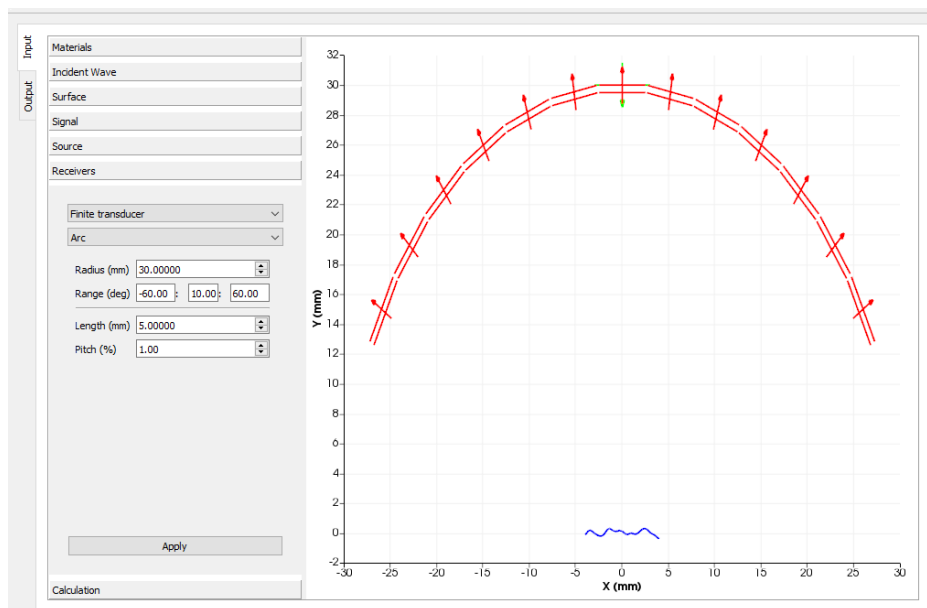


Figure 14: Arc of finite transducers located at 30mm and from -60° to 60° at intervals of 10° for the case study example.

Figure 14 also emphasises the differences in the schematic representations of the source, receivers and plane wave/transducer settings. Red double-lined units correspond to receiving transducers (also indicated by the direction of the arrows) whilst the green single-lined object represents an incident plane wave. The selection of `Single` in place of `Arc` also introduces several additional input boxes, as shown in Figure 15 where there are greyed out options if point receivers are used instead of finite transducers. As one may expect, for a single point receiver, only the point coordinates are required to be entered in millimetres.

However, for the *single* finite transducer option, the coordinates that should be entered as X and Y should define the centre of the transducer. The other three inputs also become active, and should be used to define the angle of orientation (it is recommended for this to be defined consistently

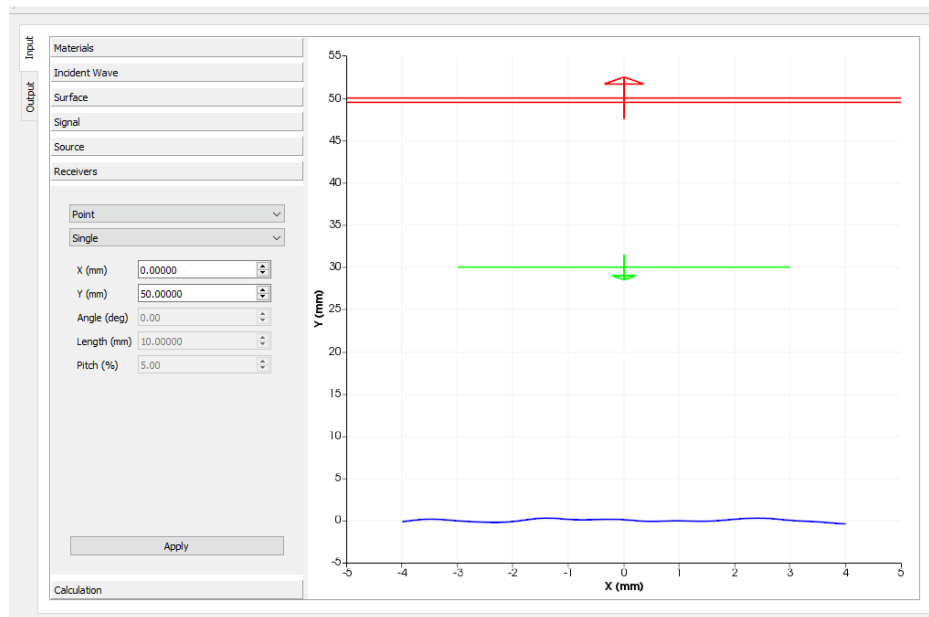


Figure 15: Single receiving finite transducer located at 50mm with length of 10mm and pitch of 5%.

with the transducer centre coordinates), length and pitch, as defined above. Note that the choice of receivers is independent of the choices made for the Source tab but it is advisable to consider this when making these selections. The angle option for the single transducer receiver also requires some attention. Due to the phase difference of 180° between a source transducer and a receiver transducer, the angles for receiving in the left half of the plane should be defined as positive (i.e. for $X < 0$), and negative for $X > 0$. For example, a single transducer receiver at $(X, Y) = (30, 30)$ would be defined with an angle of -45° .

A specific example is illustrated in Figure 16. For normal incidence, a single receiving finite transducer is located at a scattering angle of -30° and a distance of 20mm from the centre of the rough crack in Figure 16. In order to calculate the coordinates for (X, Y) , some simple trigonometry is implemented: $X = 20 \sin(30^\circ)$ and $Y = 20 \cos(30^\circ)$, giving the values shown on the left hand side of Figure 16.

2.2.7 Calculation

Once the full model has been described, the calculation of the KA reflection amplitudes may be performed. It is important to note that it is possible to toggle back and forth between all of the preceding input tabs to update them

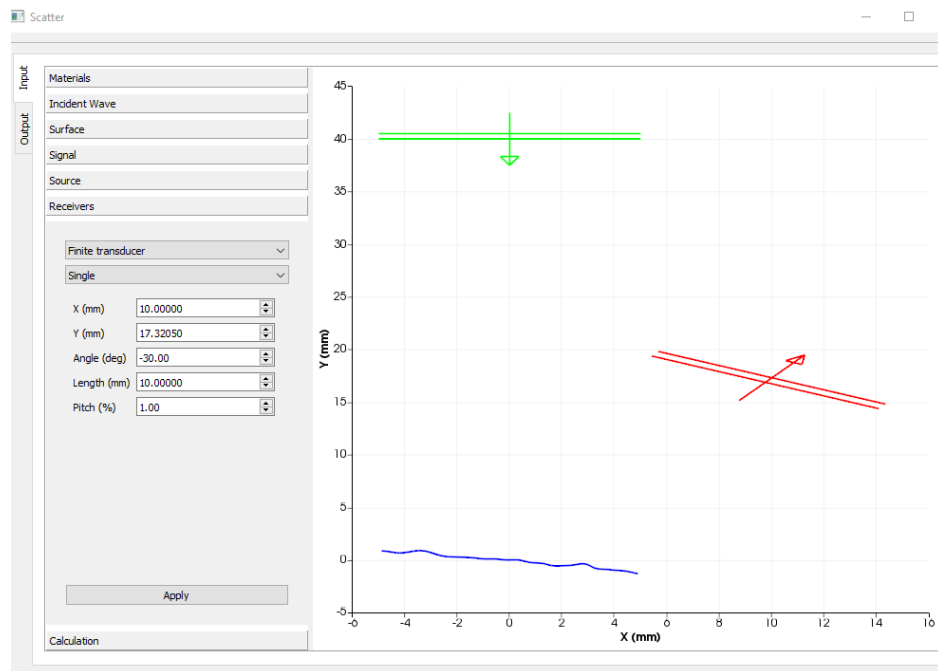


Figure 16: Single receiving finite transducer located at $(X, Y) = (10, 17.32)$, a distance of 20mm from the centre of the rough defect, Angle = -30° . The transducer length and pitch are defined in the open Receivers tab.

before clicking Compute under the Calculation tab. If any changes are made, they are only confirmed if the relevant Apply, Generate or Load Surface button is clicked. Once the user is ready, open the Calculation tab and click Compute. Although, there is a drop-down menu for the calculation type, only the KA model is installed on version 1.0.0. Similarly, only a single calculation (parametric is disabled) format is presently supported. Once the calculation has been performed, which is generally very rapid, the results are displayed under the Output tab, which is the subject of Section 2.3.

2.3 Outputs

The output tab displays the reflected amplitudes plotted in accordance with the selections made for the receivers. The pre-loaded result for the case study is shown in Figure 17, which is the same picture as in Figure 10a when the implementation of Gaussian tapering amplitude functions was discussed in Section 2.2.5. For an incident plane wave with $G_{tf} = 5\text{mm}$, and receivers defined as shown in Figure 13, the amplitudes normalised with respect to

the normal incidence case for a smooth defect of the same size, are plotted in Figure 17.

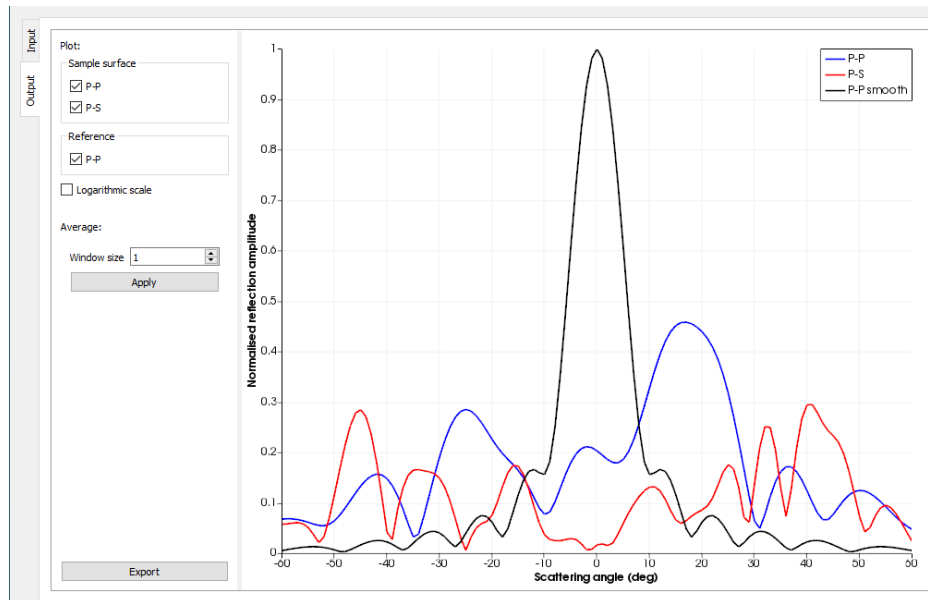


Figure 17: Normalised reflected amplitudes for P-P, P-S and for the smooth defect of the same length.

Three sets of results are produced for each surface. For P-wave incidence (as in the case study), the P-P and P-S reflected amplitudes are plotted in blue and red, respectively. The third set of results in black represents the reference case of a smooth defect, of the same length as the rough surface under investigation. For each Source type (plane wave, point source or finite transducer), all results are normalised with respect to the reflected amplitude at 0° for the smooth defect undergoing normal incidence from the same type of Source, as indicated by the peak value of unity for the black curve in Figure 17. There are three check boxes under Plot within the Output tab, and all are ticked in Figure 17. By checking or unchecking these boxes, one may plot the curves of interest. For the case of S-wave incidence, these options become S-S, S-P and S-S for the reference.

The corresponding dB results are available by checking the Logarithmic scale box, which is located just below the Reference P-P case. These results are shown in Figure 18. The same details are visible in both plots, but for low amplitude values, the dips that arise due to interference may be quite extreme for the dB plots, as illustrated for the P-S case in Figure 18 around 0° . In practice, in a scanned inspection, multiple angles are used for detection within the spread of a beam and this will mitigate sharp dips

in amplitude/intensity. Therefore, the worst case value in practice is highly likely to be better than -40dB.

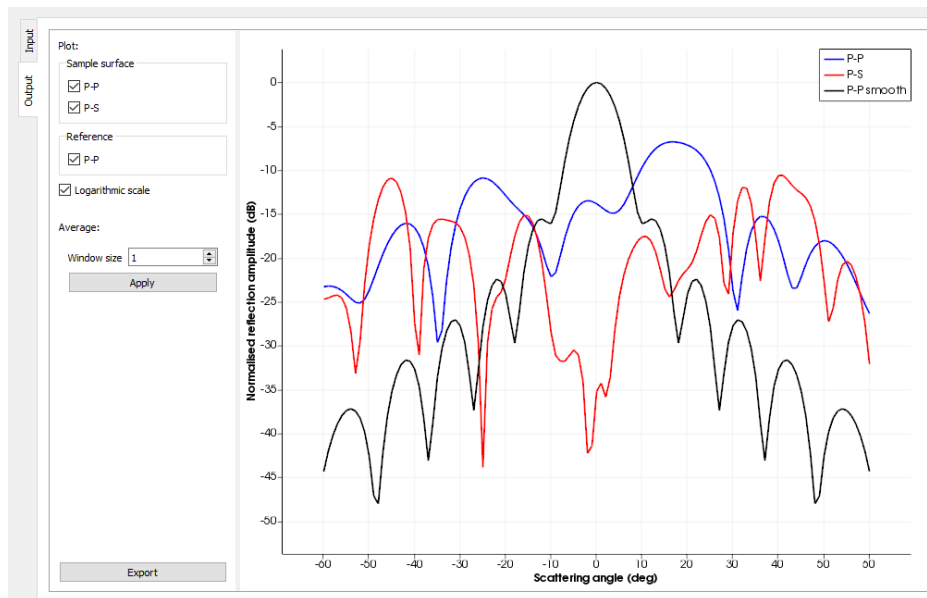
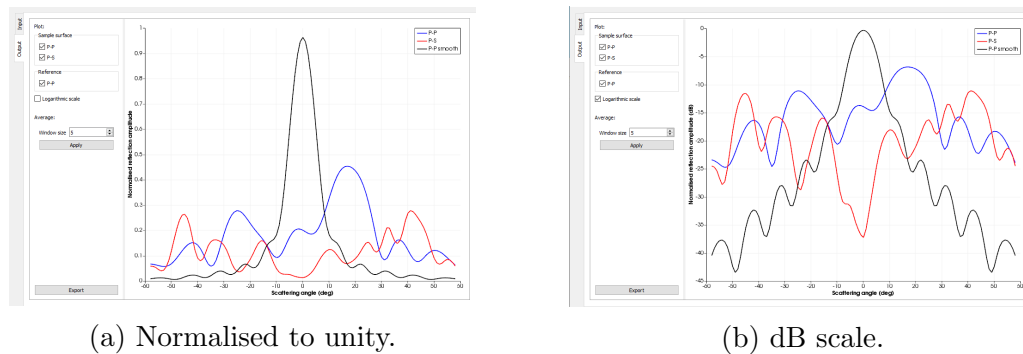


Figure 18: Normalised reflected amplitudes for P-P, P-S and for the smooth defect of the same length, on the dB scale.

Scatter includes capability for obtaining a spatial average in the frequency domain by computing the mean over a specified range of scattered angle increments for any scattering direction. To control the size of this range, the `Window size` value should be adjusted. For a chosen value m , the spatial average is calculated over values $\pm m^\circ$ either side of the plotted scattering angle. Examples for the normalised to unity and logarithmic scales are shown in Figure 19 for a window size of 5 for the case study. The effect of the spatial averaging is best understood by comparing Figures 17 and 19a and Figures 18 and 19b.

For the unity scale, some of the peaks and troughs have been reduced and smoothed by the averaging but the plots of Figures 17 and 19a are quite similar. The differences between the dB plots in Figures 18 and 19b are clearer to see, with the lowest P-S values increased to -37dB from -42dB at 0° and to -28dB from -44dB at -25° . The scattering amplitudes are averaged over 11 values (by the choice of window size = 5) rather than a single value as in Figure 18, which may provide a more realistic prediction for what an NDE engineer may observe when carrying out an inspection. The implementation of the `Window size` option is at the user's discretion, bearing in mind the primary motivation of the study. For more reliable

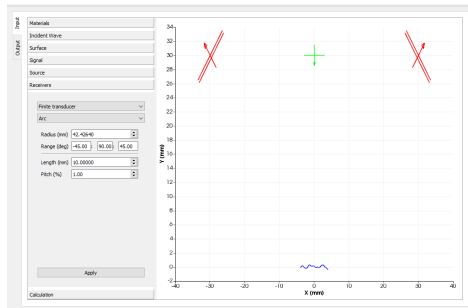
Figure 19: Spatial average window size of $\pm 5^\circ$.

understanding of interference effects in the frequency domain, minimising both Window size and the angular range step size within the Receivers tab is recommended.

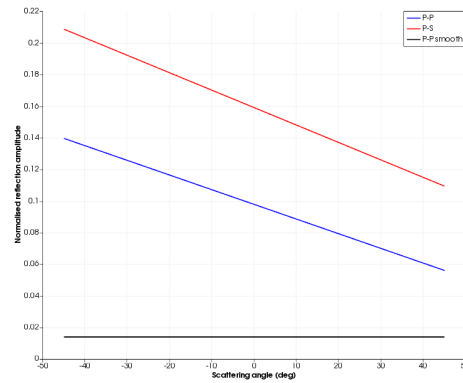
The plots may be exported by clicking the `Export` button at the bottom of the window. An additional feature is that the amplitude and coordinate values are visible by hovering over the curves with the cursor. For the case of point receivers, the most representative results are obtained by minimising the discretisation of the range of scattering angles. However, for the alternative choice of `Finite Transducer` receivers, the user is recommended to consider how to finalise their arrangement according to the desired investigation. Of course, the calculation is only run after clicking `Compute` so the user may try several different combinations of receivers before running the computation.

One may want to use only two finite transducer receivers. An example is illustrated in Figure 20 for the case of a normally incident plane wave with $G_{tf} = 5\text{mm}$ for the case study defect located at a depth of 30mm . The two receiving 10mm transducers are located at 45° , with respect to the defect, and on the surface of the component such that $Y = 30\text{mm}$ and the radius of the `Arc` is 42.4264mm , as shown in Figure 20a. The exported output results are shown in Figure 20b, which at first sight may seem unexpected being three straight lines.

The selection of two receivers means that there are two plotted amplitudes, connected by the straight lines, at -45° and 45° . The choice of finite transducer receivers, and their length of 10mm , means that these values are averaged over a relatively large number of scattering angles when compared with the results in Figure 17. Figure 20b indicates a value of 0.14 for the P-P mode at -45° whereas Figure 17 indicates a value of around 0.13 . Similarly, for 45° , Figure 20b shows a value of around 0.06 whilst Figure 17 shows



(a) Arrangement of 10mm receivers.



(b) Output for case study.

Figure 20: Two receiving finite transducers of length 10mm for case study.

around 0.08. The variation in the P-S mode values (red curves) is greater. In the event of a smaller finite transducer, the amplitude values are more comparable with the point receivers, since the averaging is over a smaller range. This is illustrated in Figure 21 for a pair of 5mm receivers.

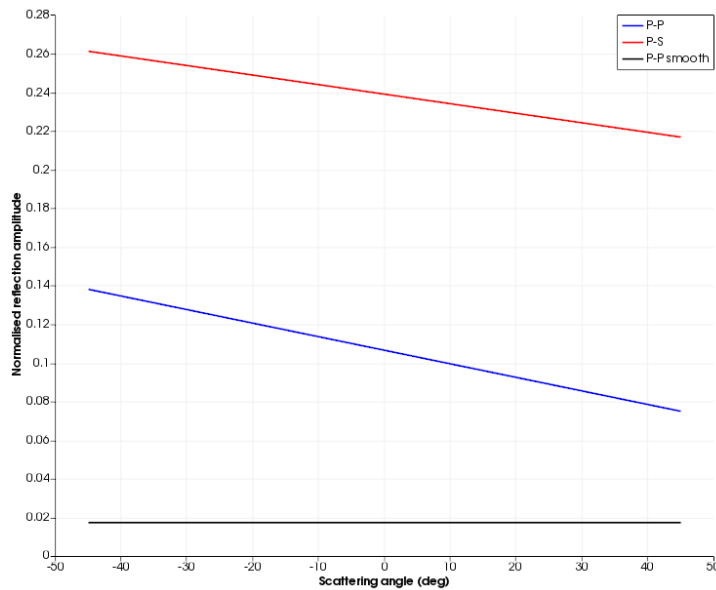


Figure 21: Two receiving finite transducers of length 5mm for case study.

2.4 Exporting output files

There are two options for exporting the scattered field results: PNG (Portable Network Graphics) or SVG (Scalable Vector Graphics) format. Both SVG and PNG files are used to store images, but SVG is a vector-based format where the image is represented by a set of mathematical shapes or figures, whereas PNG is a binary image format that uses pixels to represent the image. There are several differences between the two types:

- SVG image quality remains the same when zooming whereas PNG image quality degrades upon zooming;
- SVG images consist of paths and shapes whereas PNG images consist of pixels;
- SVG images are editable whereas PNG images cannot be edited;
- SVG is a vector-based format whereas PNG (and also GIF, JPEG) is a raster format.

The simplest way to open an SVG file is to view it using a standard web browser, such as Chrome, Firefox, Microsoft Edge or Internet Explorer. However, these options do not allow editing. Possible downloads to use the SVG format files are SVG Explorer Extension and Adobe Bridge. The reason that the bitmap image (PNG) cannot be edited is that it is composed of a fixed set of pixels, while the vector image (SVG) is composed of a fixed set of shapes. When zooming the PNG file, one reveals the pixels while upon zooming the SVG file, the shapes are preserved.

3 Underlying theory

Some of the underlying theory and modelling assumptions are presented here, including references for more detailed explanations. Figures are taken from publications for which the 2-D plane is denoted as the xz -plane, such that the x -direction is equivalent to the X -direction in Scatter, and the z -direction is equivalent to the Y -direction in Scatter.

3.1 Rough surfaces

A rough surface is usually described in terms of its deviation from a smooth reference surface, with the emphasis on two factors: the spread of heights about the mean surface and the lateral variation of these heights along the

surface. The 2-D geometry for a rough defect is illustrated in Figure 22, where the global incident and scattering angles are denoted by θ_i and θ_s , respectively. The accompanying unit wavevectors are defined as

$$\mathbf{k}^{\text{inc}} = (\sin \theta_i, -\cos \theta_i); \quad \mathbf{k}^{\text{sc}} = (\sin \theta_s, \cos \theta_s). \quad (1)$$

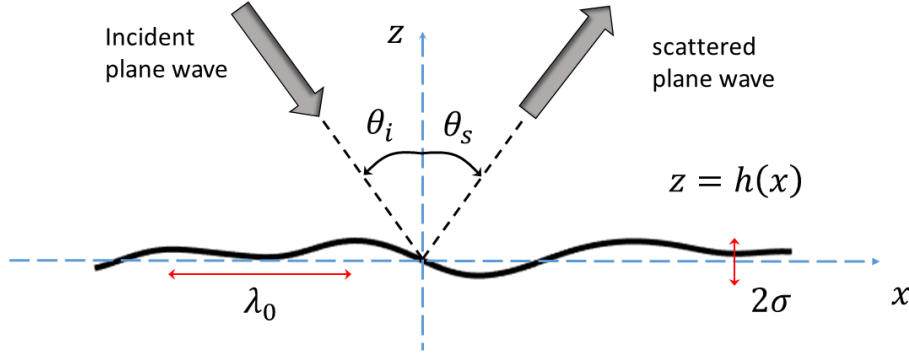


Figure 22: A plane wave scattered by a rough surface in 2-D with global incident and scattering angles θ_i , θ_s . The height data of the surface is defined by $z = h(x)$, and R is the separation between any two points of the surface.

The function $h(x)$ is defined to represent the height of the surface relative to $z = 0$, where x denotes the 1D position on this reference surface. The surface heights are described by a statistical height distribution with zero mean:

$$\langle h \rangle = \int_{-\infty}^{\infty} h p(h) dh = 0, \quad (2)$$

where $p(h) dh$ is the probability of a surface point being at a height between h and $h + dh$ away from the mean surface. The probability density function $p(h)$ for a Gaussian surface is

$$p(h) = \frac{1}{\sigma\sqrt{2\pi}} \exp\left(-\frac{h^2}{2\sigma^2}\right), \quad (3)$$

where σ is the RMS height defined (with an ergodic assumption [9]) as

$$\sigma = \sqrt{\langle h^2 \rangle} = \sqrt{\frac{1}{N} \sum_{i=1}^N h_i^2}. \quad (4)$$

This standard deviation gives us the height scale of the rough surface; the lateral variation of h is expressed using a correlation function, which is also assumed to be Gaussian here:

$$C(R) = \frac{\langle h(x) h(x+R) \rangle}{\sigma^2} = \exp\left(-\frac{R^2}{\lambda_0^2}\right). \quad (5)$$

The second statistical parameter, λ_0 , is called the correlation length, and is the distance over which the correlation function $C(R)$ falls by $1/e$. The lateral correlation length determines the statistical independence of a rough surface's peaks and troughs. The variable R is the distance between any two points on the surface, as shown in Figure 22. The analogous three-dimensional systems are illustrated in [4], where two correlation lengths are defined, in the x - and z -directions. For surfaces whose probability density function $p(h)$ is Gaussian, their gradients are also known to follow Gaussian distributions [9]:

$$p_g\left(\frac{\partial h}{\partial x}\right) = \frac{1}{\sigma\sqrt{2\pi}} \exp\left(-\frac{\left(\frac{\partial h}{\partial x}\right)^2}{2\sigma^2}\right). \quad (6)$$

In defining Gaussian distributions for the height and correlation functions used within Scatter, we follow preceding literature, including [1, 2, 4, 6, 10]. As well as the analytical benefits of using a well-understood statistical distribution, experimental evidence has indicated that rough surfaces possess Gaussian spectra when arising from natural processes, such as thermal fatigue [1]. As noted by Ogilvy [11], both statistical and experimental studies identified classes of rough surfaces for which distributions are close to Gaussian. Fatigue and corrosion measurements [12] have also supported this conjecture. The recent work [8] advocates an autoregressive method to accurately represent real rough surfaces in 3-D and recommends caution when assuming Gaussian roughness, advising that it performs well under certain conditions, but not universally. It is envisaged that additional rough surface height distributions will be incorporated within Scatter in updated versions.

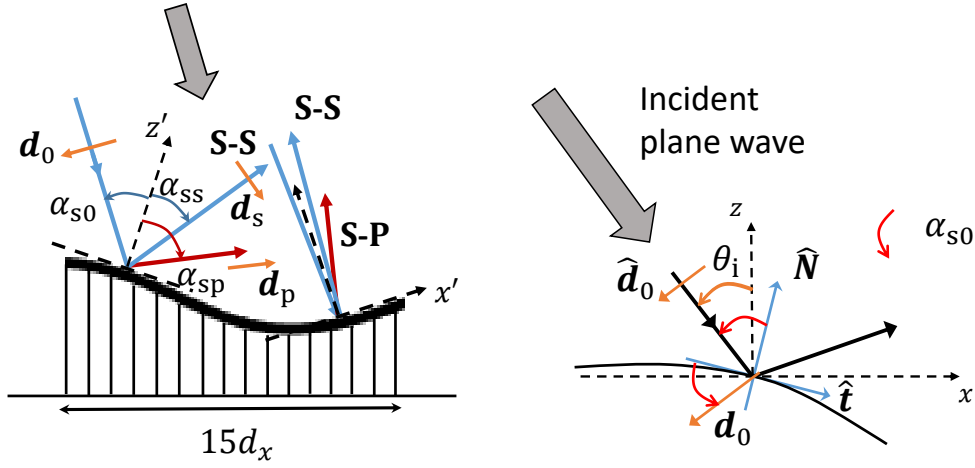
3.2 Kirchhoff Approximation

A schematic representation of Kirchhoff approximation (KA) is illustrated in Figure 23a for S-wave incidence. The motion of a single surface point is assumed to be the same as if it were part of an infinite tangential plane. The total displacement at this point is approximated as a summation of the incident shear-vertical (SV) wave and the reflected shear-shear (S-S) and

shear-longitudinal (S-P) waves:

$$\mathbf{u}^{\text{KA}} = A^{\text{sv}} (\mathbf{d}_0 + r_{\text{ss}} \mathbf{d}_s + r_{\text{sp}} \mathbf{d}_p), \quad (7)$$

where the vectors $\mathbf{d}_0, \mathbf{d}_s, \mathbf{d}_p$ are the displacement polarisation vectors and $r_{\text{ss}}, r_{\text{sp}}$ are reflection coefficients of S and P waves respectively. SV-wave incidence means that the shear wave polarisation vector is in-plane, and perpendicular to the directional vector, as indicated by the arrows in Figure 23a. For P-wave incidence, the polarisation and directional vectors are parallel.



(a) S-S and S-P wave directions and polarisation vectors are shown, as well as local coordinates x', z' for each facet of length d_x and local incident and reflected S-S and S-P angles $\alpha_{s0}, \alpha_{ss}, \alpha_{sp}$.

(b) Local tangent $\hat{\mathbf{t}}$, local normal $\hat{\mathbf{N}}$ and local and global polarisation vectors, \mathbf{d}_0 and $\hat{\mathbf{d}}_0$ respectively, for incident shear waves are shown.

Figure 23: Illustration of KA discretization and local parameters for rough surface scattering of an incident plane SV-wave.

Comparing expression (7) with the longitudinal case (see equation (8) in [2] for example), there is an additional factor A^{sv} to take account of the $\pi/2$ phase difference between polarisation and directional vectors:

$$A^{\text{sv}} = -\frac{1}{\cos \alpha_{s0}} \hat{\mathbf{d}}_0 \cdot \hat{\mathbf{t}}, \quad (8)$$

where $\hat{\mathbf{d}}_0$ is the unit polarisation vector for the global incident field and $\hat{\mathbf{t}}$ is the local unit tangent vector, defined at each point on the surface, as illustrated in Figure 23b.

The direction of the local polarisation vector \mathbf{d}_0 varies by 0 or π from that of the global polarisation vector $\hat{\mathbf{d}}_0$, which is fixed, according to the local curvature of the surface. The factor (8) accounts for this change of sign, being a normalised dot product that guarantees

$$A^{\text{sv}} \mathbf{d}_0 = \hat{\mathbf{d}}_0. \quad (9)$$

The amplitude (8) is required to maintain the sign consistency for all the waves, hence its role in the expression for the total displacement (7).

3.2.1 Reflection coefficients

The local reflection coefficients $r_{\text{ss}}, r_{\text{sp}}$ are derived following [13], assuming a traction-free boundary condition on the boundary $z' = 0$ of a local coordinate system for each facet, and therefore, each tangential plane as in Figure 23a. Thus, the coefficients depend on the local scattering angles and the wavenumbers $k_{\text{s}}, k_{\text{p}}$:

$$r_{\text{ss}} = \frac{\sin 2\alpha_{\text{s0}} \sin 2\alpha_{\text{sp}} - \kappa^2 \cos^2 2\alpha_{\text{s0}}}{\sin 2\alpha_{\text{s0}} \sin 2\alpha_{\text{sp}} + \kappa^2 \cos^2 2\alpha_{\text{s0}}}; \quad r_{\text{sp}} = \frac{-\kappa \sin 4\alpha_{\text{s0}}}{\sin 2\alpha_{\text{s0}} \sin 2\alpha_{\text{sp}} + \kappa^2 \cos^2 2\alpha_{\text{s0}}}, \quad (10)$$

where κ is the ratio of shear to longitudinal wavenumbers. Analogous reflection coefficients for P-wave incidence are published in [2, 4].

There is a crucial difference between the incident shear and incident longitudinal cases that underpins much of the contrast in the scattering behaviour. The mode-converted reflected angle, α_{sp} , can become complex since it is defined by

$$\frac{\sin \alpha_{\text{s0}}}{\sin \alpha_{\text{sp}}} = \frac{1}{\kappa}; \quad \kappa = \frac{k_{\text{s}}}{k_{\text{p}}} > 1. \quad (11)$$

Thus, there is a critical incident angle $\alpha_{\text{s0}} = \alpha_{\text{crit}}$ defined by

$$\alpha_{\text{crit}} = \sin^{-1} \left(\frac{1}{\kappa} \right). \quad (12)$$

The analogous mode-converted P-S case for longitudinal incidence shares a similar condition to (11), but with the reciprocal ratio of sines, ensuring that α_{ps} is always real. Note that in (11), a condition is defined for κ which is true for most media, and all that are relevant for ultrasonic NDE. As an example, aluminium typically has $\kappa \simeq 2$, which determines a critical incident angle of $\alpha_{\text{crit}} \simeq 30^\circ$ for shear wave incidence.

In the event of $\alpha_{\text{s0}} > \alpha_{\text{crit}}$, the reflected S-P wave propagates parallel to the surface with exponentially decaying amplitude relative to the depth of

the material, i.e. surface wave mode-conversion. The mode conversion is complicated further by the roughness of the surface whose undulations result in additional multiple scattering of the surface wave. Surface waves and multiple scattering are not accounted for by KA, although a correction to the contribution to the total displacement at each facet of the discretisation was implemented here. Facets where surface wave mode conversion occurs are identified within the Scatter codes, i.e. when the local angle

$$\alpha_{s0} > \alpha_{\text{crit}} \implies \alpha_{\text{sp}} > \pi/2,$$

and an adjustment to the local reflection coefficients $r_{\text{ss}}, r_{\text{sp}}$ is made [13], p.179:

$$\begin{aligned} r_{\text{ss}} &= -\exp(-2i\xi); \\ r_{\text{sp}} &= \frac{\exp(-i\xi + \tau k_s) \sin 4\alpha_{s0}}{\sqrt{\kappa^2 \cos^4(2\alpha_{s0}) + 4(\kappa^2 \sin^2(\alpha_{s0}) - 1) \sin^2(2\alpha_{s0}) \sin^2(\alpha_{s0})}}, \end{aligned} \quad (13)$$

where the parameters ξ, τ are introduced for complex α_{sp} , with the polarization vector \mathbf{d}_p in (7) changed accordingly, with $\gamma = \arg(\alpha_{\text{sp}})$:

$$\begin{aligned} \tan \xi &= \frac{2\sqrt{(\kappa^2 \sin^2 \alpha_{s0} - 1)} \sin 2\alpha_{s0} \sin \alpha_{s0}}{\kappa \cos^2 2\alpha_{s0}}, \\ \tau &= \frac{\sinh \gamma}{\sqrt{\sinh^2 \gamma + \cosh^2 \gamma}}. \end{aligned} \quad (14)$$

3.3 Formulation of scattering problem

The total displacement field is given by

$$\mathbf{u} = \mathbf{u}^{\text{sc}} + \mathbf{u}^{\text{inc}},$$

with the scattered field represented by the elastodynamic Helmholtz integral formula given by Ogilvy [9] p.136, and Achenbach *et al.* [14], as well as recent publications [2, 4]:

$$u_k^{\text{sc}}(\mathbf{R}) = \int_{\mathcal{S}(\mathbf{r})} \Sigma_{ijk}(|\mathbf{R} - \mathbf{r}|) u_i(\mathbf{r}) n_j(\mathbf{r}) d\mathcal{S}(\mathbf{r}), \quad (15)$$

where Σ_{ijk} is Green's stress tensor, \mathbf{R} is the location of the observation point, \mathbf{r} is a point on the rough surface $\mathcal{S}(\mathbf{r})$, \mathbf{n} is the outward unit normal vector to the surface and $u_i(\mathbf{r})$ is the i th component of the KA boundary

displacement (7). Note that for the 2-D case, the $k = 2$ component of scattered displacement u_k^{sc} is zero and the dummy indices $i, j \neq 2$ with the index values 1 and 3 corresponding to the x and z directions respectively (see Figure 22).

Using far-field assumptions [10] $R \gg r$ and $k_\alpha R \gg 1$, where the index α denotes the incident wave-type i.e. shear wave in this case, (15) may be simplified as

$$\mathbf{u}^{\text{sc}}(\mathbf{R}) = -ik_\beta \sqrt{\frac{2\pi i}{k_\beta}} \int_{\mathcal{S}_0} \frac{e^{ik_\beta D}}{4\pi\sqrt{D}} \mathbf{U}_{s\beta}(\mathbf{D}, \kappa) d\mathcal{S}_0. \quad (16)$$

Here, the integration over the rough surface has been converted to one over the mean line \mathcal{S}_0 (i.e. $z = 0$) by using

$$nd\mathcal{S} \approx \mathbf{N}_0 d\mathcal{S}_0, \quad \mathbf{N}_0 = -\mathbf{i} \frac{\partial h}{\partial x} + \mathbf{k}, \quad (17)$$

where \mathbf{i} and \mathbf{k} are the unit orthonormal basis vectors. In effect, the integration may be performed over small rectangular elements of the rough surface, parallel to the local tangent [9].

Note also the use of the vector $\mathbf{D} = \mathbf{R} - \mathbf{r}$ in (16), with associated magnitude D and unit vector $\hat{\mathbf{D}}$. Since R represents the far-field, further approximations may be used, as with the stationary phase approach of [4, 6], but for KA reflection amplitude evaluation, it remains to integrate (16) numerically, which Scatter performs for any specified finite surface. The KA appears within the boundary displacement term $\mathbf{U}_{s\beta}$ where the index β denotes the scattered wave-type, which can be shear s or longitudinal, p :

$$\mathbf{U}_{\text{sp}}(\hat{\mathbf{D}}, \kappa) = \left[(\mathbf{u}^{\text{KA}} \cdot \mathbf{N}_0) \left(1 - \frac{2}{\kappa^2} \right) + \frac{2}{\kappa^2} (\mathbf{u}^{\text{KA}} \cdot \hat{\mathbf{D}}) (\mathbf{N}_0 \cdot \hat{\mathbf{D}}) \right] \hat{\mathbf{D}} \quad (18)$$

$$\mathbf{U}_{\text{ss}}(\hat{\mathbf{D}}, \kappa) = (\mathbf{N}_0 \cdot \hat{\mathbf{D}}) \mathbf{u}^{\text{KA}} + (\mathbf{u}^{\text{KA}} \cdot \hat{\mathbf{D}}) \mathbf{N}_0 - 2 (\mathbf{u}^{\text{KA}} \cdot \hat{\mathbf{D}}) (\mathbf{N}_0 \cdot \hat{\mathbf{D}}) \hat{\mathbf{D}}. \quad (19)$$

The functions $\mathbf{U}_{s\beta}(\hat{\mathbf{D}}, \kappa)$ depend on the local incident and scattered angles and the roughness of the surface in the terms \mathbf{u}^{KA} in equation (7), \mathbf{N}_0 in equation (17) and $\hat{\mathbf{D}}$, as well as the physical parameters in the wavenumber ratio κ . The standard bulk wave equations relating wavenumber to wave-speed are expressed as

$$k_s = \frac{\omega}{c_s} = \omega \sqrt{\frac{2\rho(1+\nu)}{E}}; \quad k_p = \frac{\omega}{c_p} = \omega \sqrt{\frac{\rho(1+\nu)(1-2\nu)}{E(1-\nu)}}. \quad (20)$$

It follows that equation (16) is actually a sum of two integrals:

$$u^{\text{sc}}(\mathbf{R}) = \sqrt{\frac{2\pi k_p}{i}} \int_{S_0} \frac{e^{ik_p D}}{4\pi\sqrt{D}} \mathbf{U}_{\text{sp}} dS_0 + \sqrt{\frac{2\pi k_s}{i}} \int_{S_0} \frac{e^{ik_s D}}{4\pi\sqrt{D}} \mathbf{U}_{\text{ss}} dS_0. \quad (21)$$

Numerical integration of (21) is carried out for specific realisations of rough surfaces. The rough surfaces are discretised into small rectangular facets of length d_x , and the orientation of each facet is given by the surface slope at its midpoint. Equation (21) is then written as the summation of contributions from N facets:

$$\begin{aligned} u^{\text{sc}}(\mathbf{R}) = & \sqrt{\frac{2\pi k_p}{i}} \sum_{n=1}^N A_n \int_{S_n} \frac{e^{ik_p D_n} e^{ik_s \mathbf{r} \cdot \mathbf{k}^{\text{inc}}}}{4\pi\sqrt{D_n}} \mathbf{U}_{\text{sp}} dS_n \\ & + \sqrt{\frac{2\pi k_s}{i}} \sum_{n=1}^N A_n \int_{S_n} \frac{e^{ik_s (D_n + \mathbf{r} \cdot \mathbf{k}^{\text{inc}})}}{4\pi\sqrt{D_n}} \mathbf{U}_{\text{ss}} dS_n. \end{aligned} \quad (22)$$

Note that each facet is assigned a vector $\mathbf{D}_n = \mathbf{R} - \mathbf{r}_n$, where n denotes the facet number. Additional details may be found in [2, 3, 10].

For incident plane waves, the amplitude term A_n in (22) is defined in one of two ways:

$$A_n = 1 \quad (\text{pure}); \quad A_n = \exp(-x_n^2/w^2) \quad (\text{Gaussian tapered}), \quad (23)$$

depending on the type of plane wave excitation (x_n denotes the centre of the n th facet). A pure plane wave excitation is assumed to be of constant amplitude $A_n = 1$, but with varying phase. For a finite defect, whose length is defined by L , an additional refinement to exclude the effect of the tips may be investigated. In this case, a tapered plane wave with a Gaussian amplitude profile is applied, the details of which are explained in detail in [2, 3, 15].

4 Tutorial case studies

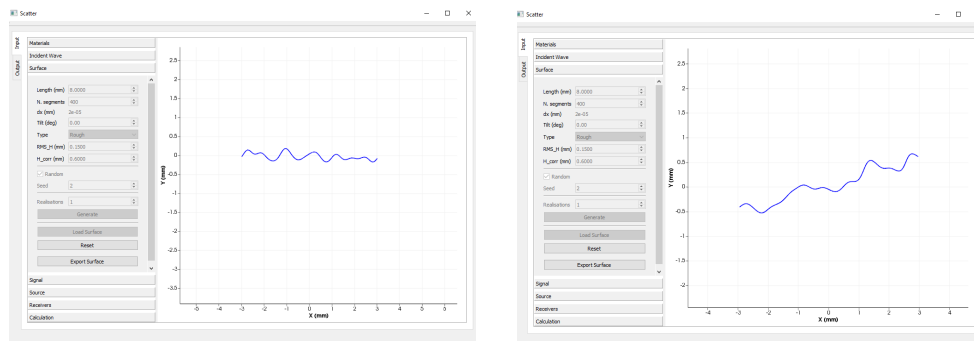
The three rough surface datasets provided separately with Scatter were generated using this software package and exported as CSV files. Three distinct types of defect are considered:

- No tilt;
- Tilted by 10° in an anticlockwise direction;
- Tilted by 10° in a clockwise direction (i.e. -10°).

In this section, tutorials for various cases of P- and S-wave incidence are explained step-by-step, for each type of excitation and receiver, from the importing step all the way through to interpreting the scattering results. All of these tutorial examples assume the preloaded stainless steel material parameter values, as seen when opening Scatter.

4.1 Defect 1 (no tilt)

Begin by opening the Surface tab, and clicking Reset if necessary, which enables the Load Surface option. Import the dataset1 file from the folder it was saved in. The surface in the main window will then be replaced by defect 1, which is a 6mm rough crack, with $\sigma = 0.1\text{mm}$ and $\lambda_0 = 0.4\text{mm}$. The surface discretization stepsize is $10\mu\text{m}$, having set the number of segments to 600 when generating the surface.



(a) Magnification of defect 1.

(b) Magnification of defect 2.

Figure 24: Tutorial defect examples. Both have length 6mm, with $\sigma = 0.1\text{mm}$ and $\lambda_0 = 0.4\text{mm}$. The surface discretization stepsize is $10\mu\text{m}$.

A magnified version of the defect is shown in Figure 24a, having used the zooming capability in the main Scatter graphical window. Both P- and S-wave incidence are considered for this example, but the former case is investigated first by clicking on the Incident Wave tab and then choosing compression waves and selecting Apply. For Signal, change the frequency to 2.25MHz, click Apply and then open the Receivers tab. For the defect 1 examples, a fixed choice of receivers is used, and the Source options are varied in the results that follow. After opening the Receivers tab, ensure that Point and Arc are selected and change the Radius to 30mm, leaving the Range to be -60° to 60° in increments of 1° .

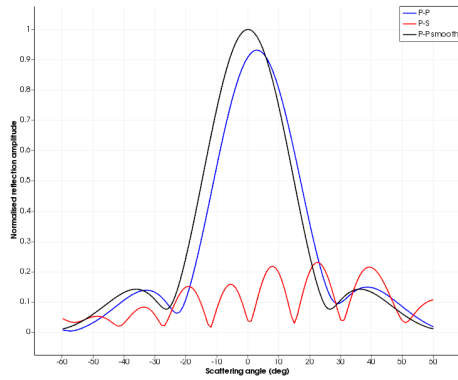
The results for the following Source settings for P-wave incidence with 0 angle of incidence are then illustrated in Figure 25:

- Plane wave with $G_{tf} = 0$ (i.e. a pure plane wave);
- Plane wave with $G_{tf} = 3\text{mm}$;
- Plane wave with $G_{tf} = 3\text{mm}$ in dB (by ticking the logarithmic scale box);
- Point source located at $(X, Y) = (0, 30\text{mm})$ with amplitude = 1;
- Point source located at $(X, Y) = (0, 60\text{mm})$ with amplitude = 1.

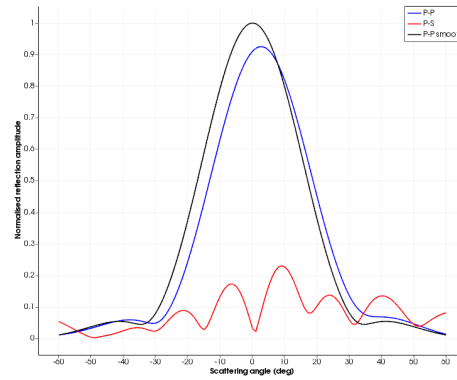
After opening the `Source` tab, updating the plane wave or point source specifications and selecting `Apply`, open the `Calculation` tab and press `Compute`. Navigate to the `Output` tab to compare results with those shown below in Figure 25 for each of the five cases. When moving from one example to the next, changing only the `Source` inputs each time is sufficient, since all other parameter settings are retained for this tutorial. Remember that you may need to zoom in or out to obtain exactly the same view illustrated here. For examples 25b and 25c, there is no need to repeat the calculation; simply tick the `Logarithmic scale` box on the `Output` tab.

All five examples of `Source` settings are illustrated in turn in Figures 25a-25e. The comparison of parts (a) and (e) are particularly illustrative, since they show the similarity between a pure plane wave excitation and a point source located at distance from the rough crack. At first sight, the scattered fields appear indistinguishable, but on closer inspection, it is possible to discern small differences, such as the slightly lower dip for the P-S mode at around 15° in Figure 25a compared with Figure 25e. The use of a plane wave with a Gaussian tapered spatial envelope of halfwidth 3mm, as shown in Figure 25b, produces a result with qualitative similarities to Figures 25a, 25c, 25d. The P-P results look very similar with the only difference being a pair of lobes observed at $\theta_s = -30^\circ$ and 40° for all cases except for the $G_{tf} = 3\text{mm}$ example. The physical interpretation of this result is that the Gaussian tapered plane wave is not interacting with the ends of the crack, so some of the interference effects are not being accounted for in the scattered field.

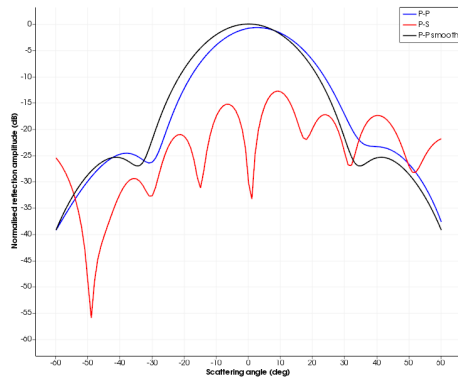
The dB plot for $G_{tf} = 3\text{mm}$ in Figure 25c indicates that the P-P result for the rough defect (blue curve) is fairly comparable with the smooth defect result (black curve). There is a small reduction in peak amplitude, and a slight shift away from the normal incidence backscattered direction. At the relatively low frequency of 2.25MHz, with an incident wavelength of 2.64mm, the roughness parameters of $\sigma = 0.1\text{mm}$ and $\lambda_0 = 0.4\text{mm}$ appear to have relatively little effect on the ultrasonic reflection. The insonification



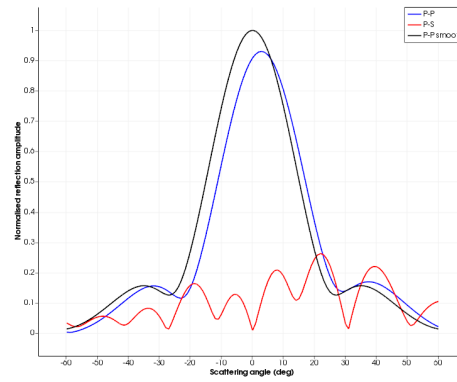
(a) Pure plane wave ($G_{tf} = 0$).



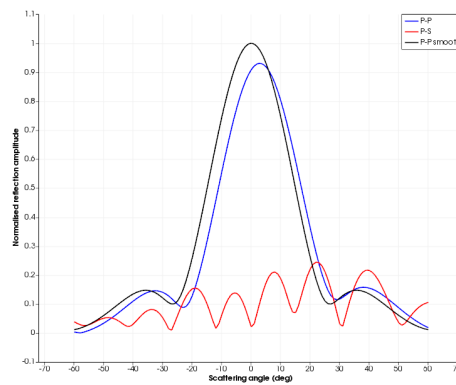
(b) Plane wave with $G_{tf} = 3\text{mm}$.



(c) Same as (b) in dB.



(d) Point source at (0,30mm).



(e) Point source at (0,60mm).

Figure 25: Defect 1 insonified by P-wave excitation with centre frequency 2.25MHz.

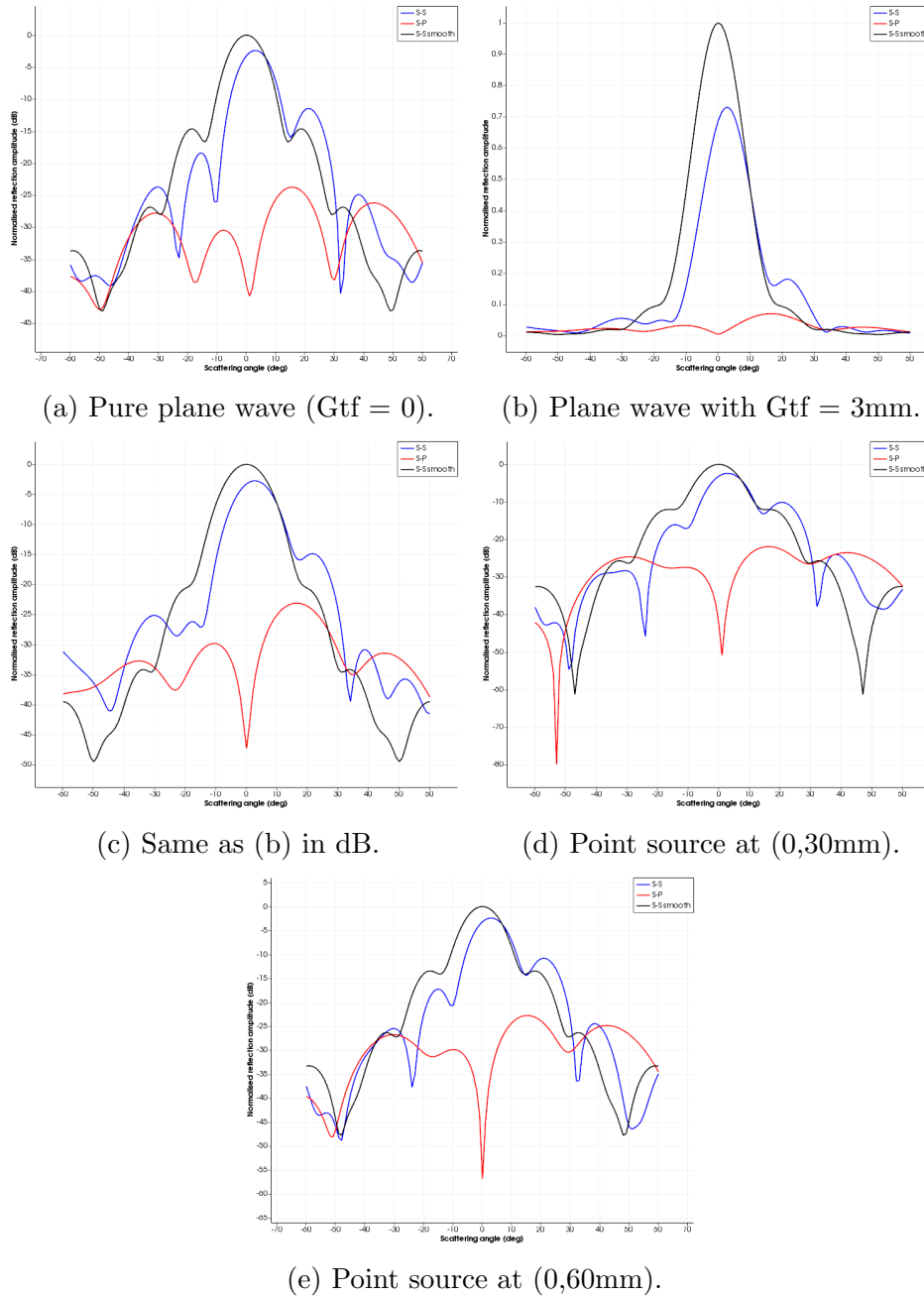


Figure 26: Defect 1 insonified by S-wave excitation with centre frequency 2.25MHz.

by shear waves at the same frequency, with wavelength 1.44mm, will show a greater variation in reflection behaviour when comparing the smooth and rough defects.

To observe this, click on the `Incident wave` tab and select shear waves and click `Apply`. Then everything can be retained except for the `Source` settings. The same five settings as listed above for the P-wave case should be calculated in turn, to produce the results shown in Figure 26. For the shear wave cases, the dB plots are shown for all cases, except for Figure 26b for the plane wave with $G_{tf} = 3\text{mm}$.

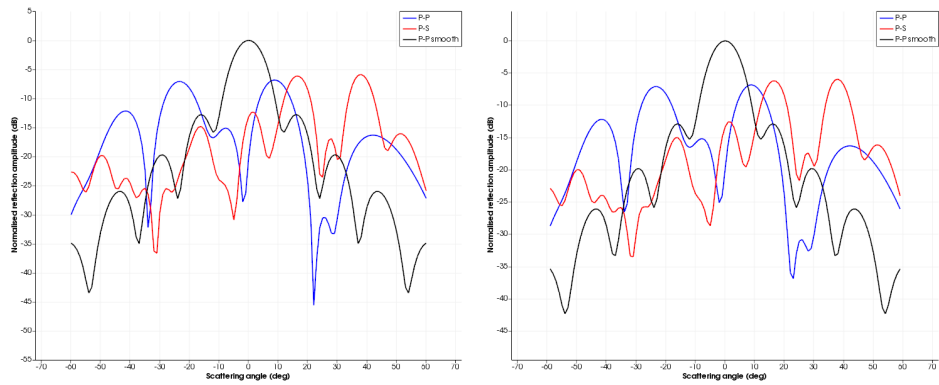
4.2 Defect 2 (tilted in anticlockwise direction)

Defect 2 was generated almost identically to defect 1. All physical parameters were kept the same except that the tilt angle was set to 10° . In order to import it, open the `Surface` tab, click `Reset` again and `Load Surface`, navigating to where the `dataset2` file was saved. If you are completing this tutorial for defect 2 on a different occasion from defect 1, the `Load Surface` tab will be active after opening `Scatter`, and so using the `Reset` option would be unnecessary. Since the roughness parameters were maintained at $\sigma = 0.1\text{mm}$ and $\lambda_0 = 0.4\text{mm}$, the two rough surfaces belong to the same class, but possess different geometries, as is clear when comparing the two defects directly (see Figures 24a and 24b).

In this tutorial, the frequency is increased to 5MHz and the use of the `Window size` option, within the `Output` tab, is illustrated. As mentioned in Section 2.3, `Scatter` includes capability for obtaining a spatial average in the frequency domain by computing the mean over a specified range of scattered angle increments for any scattering direction. To control the size of this range, the `Window size` value should be adjusted. For a chosen value m , the spatial average is calculated over values $\pm m^\circ$ either side of the plotted scattering angle.

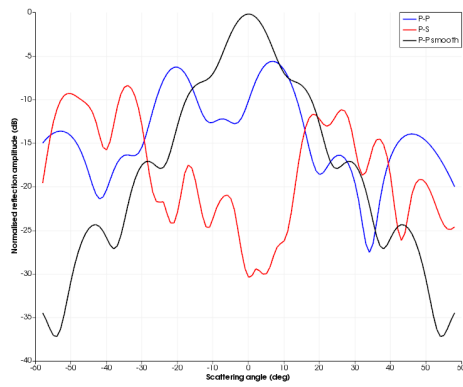
Firstly, the `Incident Wave` tab should be opened, and compression waves selected. Then, open `Signal` and enter the value 5MHz and click `Apply`. For the `Source`, choose a pure plane wave ($G_{tf} = 0$) but adjust the angle to 30° , before clicking on `Apply`. For the `Receivers` tab, update the settings to be an arc of point receivers ranging from -60 to 60° in intervals of 1° , with a `Radius` value of 30mm. Once everything has been applied, open `Calculation` and press `Compute`. Tick the `Logarithmic scale` box in the `Output` tab and compare results with those displayed in Figure 27a.

Now update the `Window size` box value to 3, click `Apply`, and check that your results match Figure 27b. Before moving onto a point source excitation, it is worthwhile comparing the results of Figures 27a and 27b

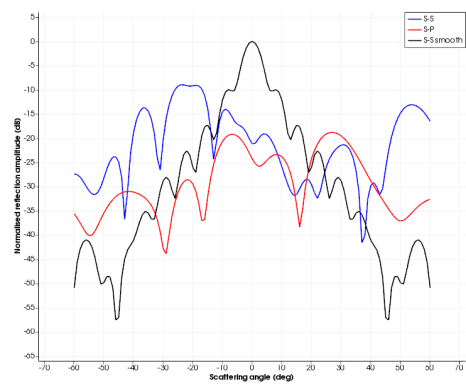


(a) Pure plane P-wave at 30° .

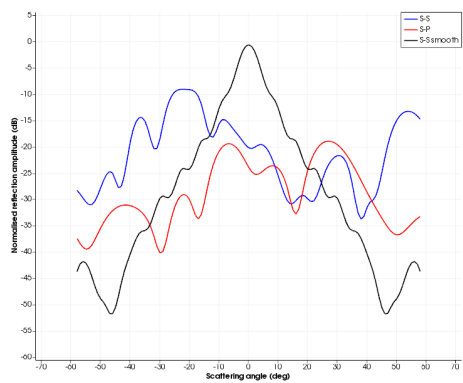
(b) panel (a) with Window size = 3.



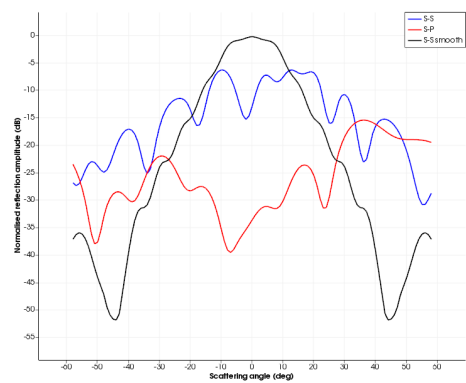
(c) Point source P-wave at (0,20).



(d) Pure plane S-wave at 30° .



(e) panel (d) with Window size = 5.



(f) Point source S-wave at (0,20).

Figure 27: Defect 2 insonified by P- and S-wave excitations with centre frequency 5MHz. Panel (f) has Window size = 5.

more carefully. The two dominant peaks for the P-P mode are at the same scattering angle values of 9° and -23° (check this by hovering over the output results with the cursor) but with slightly lower values: -6.89 dB compared with -6.81dB and -7.15dB compared with -7.08dB, respectively. More notable differences are the dips at 22° , -2° and -34° , which are all less pronounced for the window size setting of 3.

Now retrace your steps to the `Source` tab, and update the settings to a point source positioned at $(X, Y) = (0, 20\text{mm})$, with amplitude set to 1. Click `Apply` and then compute the result, which should look like Figure 27c, once the `Window size` box value has been increased to 5. For a better understanding of how the `Window size` option may be utilised, it is recommended to compare various values.

Now examples with shear wave excitations for defect 2 are considered. After updating the `Incident wave` setting, navigate to the `Source` tab and choose a pure plane wave ($G_{tf} = 0$) incident at 30° . Click `Apply`, proceed to the `Calculation` tab and compute. The result should agree with Figure 27d for `window size = 1`, and by increasing the `Window size` value to 5, should match Figure 27e. Finally, consider a point source for a shear wave, located at $(X, Y) = (0, 20\text{mm})$. The results for a `Window size` value of 5 are shown in Figure 27f, with the same receiver settings as for the other defect 2 cases considered.

4.3 Defect 3 (tilted in clockwise direction)

For the final tutorial example, the defect has been tilted in the clockwise direction, through -10° , and was defined using different roughness parameter values, length and discretization step size. Defect 3 is a 10mm rough crack, with $\sigma = 0.15\text{mm}$ and $\lambda_0 = 0.6\text{mm}$. The surface discretization step-size is $12.5\mu\text{m}$, having set the number of segments to 800 when generating the surface. Defect 3 was shown in Figure 16, when discussing the options associated with finite transducers for the `Receivers` tab.

As for the previous two examples, begin by opening the `Surface` tab and click on `Load Surface`. Import `dataset3.csv` from where it was saved. Once again, both P- and S-wave incidence are considered but begin with the P-wave case, using the `Incident Wave` tab. Open the `Signal` tab, and ensure that the frequency is set to 5MHz. For the `Source` tab, choose the `Finite transducer` option from the drop-down menu and position the centre of the transducer at $(X, Y) = (0, 40\text{mm})$. Set the angle of incidence to be 0° and the length to be 10mm, before clicking on `Apply`.

After opening the `Receivers` tab, opt for `Finite transducer` and `Single` from the two drop-down menus. This combination gives the user five

parameter values to enter:

- X (mm): 0mm;
- Y (mm): 40mm;
- Angle (deg): 0;
- Length (mm): 10mm;
- Pitch (%): 1.

By choosing the values provided, a simple pulse-echo inspection for normal incidence is simulated. The single receiving transducer is seen to overlay the source transducer, with the same location and length selected. The reflected signal is averaged over the length of the transducer, which is discretized according to the choice of `Pitch`, the lower this number, the more reliable the calculation. After clicking `Apply`, open the `Calculation` tab and press `Compute`. The output should match the results shown in Figure 28a.

Figure 28b was produced with nearly all of the same `Input` settings, with a change to the `Receivers` tab only. In place of selecting `Single` from the drop-down menu, opt for `Arc` and set the four parameter values as follows:

- Radius (mm): 40;
- Range (deg): $-60 : 15 : 60$;
- Length (mm): 10;
- Pitch (%): 1.

The updated arc of receivers, located 40mm from the centre of the rough crack at 15° intervals, includes the single receiver result from the pulse-echo set-up in Figure 28a, and this can be confirmed by comparing the results at 0° for both Figures 28b and 28a. By ticking the `Logarithmic scale` box, the amplitudes are obtained in dB, and these are shown in Figure 28c.

The P-P result for 0° incidence indicates a peak between 0° and 30° , so it is natural to consider alternative angles of incidence. Open the `Source` tab and update the `Angle` to 15° , but retain the same length of 10mm. The centre of the finite transducer can be calculated using simple trigonometry for a specified source-crack distance. Choosing 40mm as in the previous examples, the `X` coordinate is calculated as $-40 \sin(15^\circ)$ and the `Y` coordinate as $40 \cos(15^\circ)$, giving -10.35276 and 38.63703, respectively. The resulting set-up is illustrated in Figure 29.

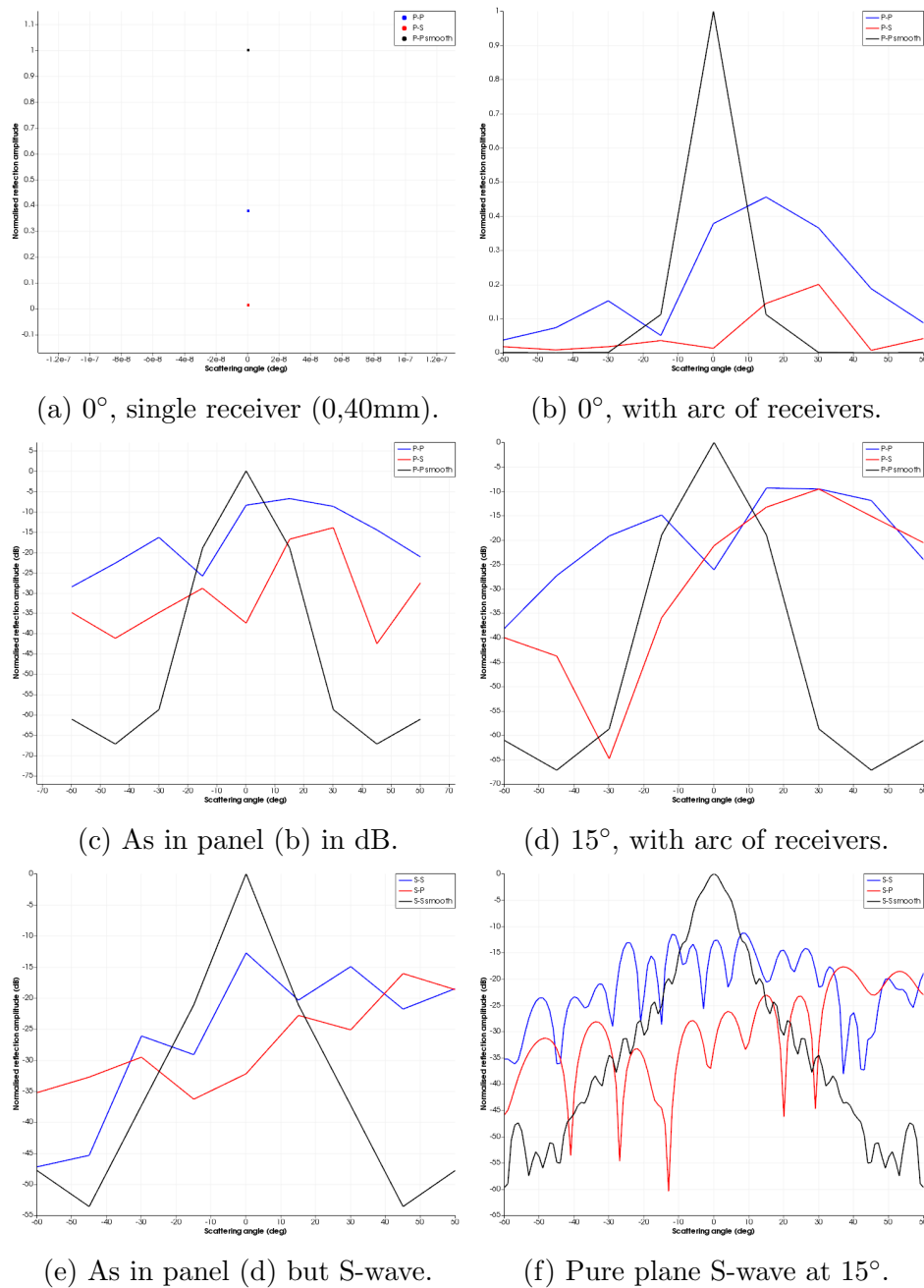


Figure 28: Defect 3 insonified by P- and S-wave finite transducer excitations with centre frequency 5MHz. Panels (a)-(d) show the P-wave case with a source of length 10mm and pitch 1%. Finite transducer receivers, with the same length and pitch as the source, are implemented for panels (a)-(e) with a single receiver in (a) and an arc from -60° to 60° in 15° intervals for the others. Panels (e) and (f) show S-wave incidence; (f) shows a plane wave with $G_{tf} = 6\text{mm}$ and a receiving arc of point receivers at 1° intervals.

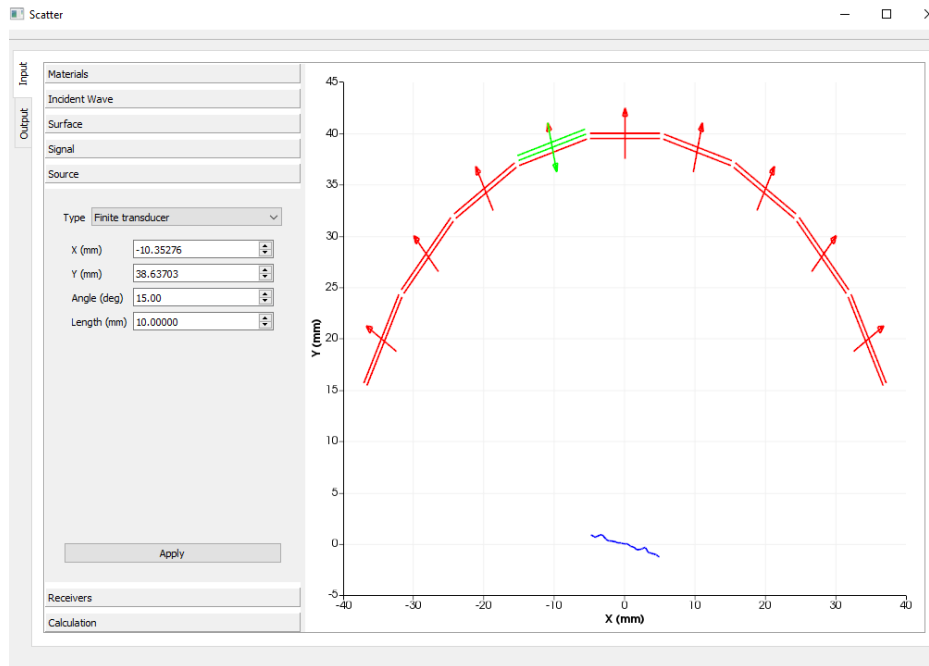


Figure 29: Set-up for example of Figure 28d, with incident P-wave finite transducer of length 10mm, angle 15° and a set of finite transducer receivers positioned at 15° intervals on an arc of radius 40mm.

After clicking `Apply`, compute the scattered field and compare results with those shown in Figure 28d. It is important to note that the use of an arc of nine finite transducers produces reflection amplitudes at nine locations in the scattered field. Peaks and troughs in amplitude may be present at scattering amplitudes between these locations, but the values are obtained by averaging over finite transducers of length 10mm with 1% pitch. Exactly the same set up may be used for incident shear waves by opening the `Incident Wave` tab and selecting shear waves, before computing. The results are shown in Figure 28e. To check the scattered field between the transducer locations, it is interesting to consider a plane wave excitation. Open the `Source` tab and select plane wave and set `Angle = 15^\circ` and `Gtf = 6mm`. Open the `Receivers` tab, and update the first drop-down menu to `Point` and change the increment of the `Arc` range to 1° . After computing, compare the results with Figure 28f.

Bibliography

- [1] J. Zhang, B.W. Drinkwater, and P.D. Wilcox. Longitudinal wave scattering from rough crack-like defects. *IEEE transactions on Ultrasonics, Ferroelectrics, and Frequency control*, 58(10):2171–2180, 2011.
- [2] F. Shi, W. Choi, M.J.S. Lowe, E.A. Skelton, and R.V. Craster. The validity of Kirchhoff theory for scattering of elastic waves from rough surfaces. *Proceedings of the Royal Society A: Mathematical, Physical and Engineering Sciences*, 471(2178):20140977, 2015.
- [3] S.G. Haslinger, M.J.S. Lowe, P. Huthwaite, R.V. Craster, and F. Shi. Appraising Kirchhoff approximation theory for the scattering of elastic shear waves by randomly rough defects. *Journal of Sound and Vibration*, 460:114872, 2019.
- [4] F. Shi, M.J.S. Lowe, X. Xi, and R.V. Craster. Diffuse scattered field of elastic waves from randomly rough surfaces using an analytical Kirchhoff theory. *Journal of the Mechanics and Physics of Solids*, 92:260–277, 2016.
- [5] J.B. Elliott, M.J.S. Lowe, P. Huthwaite, R. Phillips, and D.J. Duxbury. Sizing subwavelength defects with ultrasonic imagery: An assessment of super-resolution imaging on simulated rough defects. *IEEE transactions on Ultrasonics, Ferroelectrics, and Frequency control*, 66(10):1634–1648, 2019.
- [6] S.G. Haslinger, M.J.S. Lowe, P. Huthwaite, R.V. Craster, and F. Shi. Elastic shear wave scattering by randomly rough surfaces. *Journal of the Mechanics and Physics of Solids*, 137:103852, 2020.
- [7] S.G. Haslinger, M.J.S. Lowe, R.V. Craster, P. Huthwaite, and F. Shi. Prediction of reflection amplitudes for ultrasonic inspection of rough planar defects. *Insight-Non-Destructive Testing and Condition Monitoring*, 63(1):28–36, 2021.
- [8] W. Choi, F. Shi, M.J.S. Lowe, E.A. Skelton, R.V. Craster, and W.L. Daniels. Rough surface reconstruction of real surfaces for numerical simulations of ultrasonic wave scattering. *NDT & E International*, 98: 27–36, 2018.
- [9] J.A. Ogilvy. *Theory of wave scattering from random rough surfaces*. CRC Press, 1991.

-
- [10] J. A. Ogilvy and I. D. Culverwell. Elastic model for simulating ultrasonic inspection of smooth and rough defects. *Ultrasonics*, 29(6):490–496, 1991.
- [11] J.A. Ogilvy. Theoretical comparison of ultrasonic signal amplitudes from smooth and rough defects. *NDT & E International*, 19:371–385, 1986.
- [12] J. Zhang, B.W. Drinkwater, and P.D. Wilcox. Effect of roughness on imaging and sizing rough crack-like defects using ultrasonic arrays. *IEEE transactions on Ultrasonics, Ferroelectrics, and Frequency control*, 59(5): 939–948, 2012.
- [13] J.D. Achenbach. *Wave Propagation in Elastic Solids*. North-Holland Publishing Company/American Elsevier, 1973.
- [14] J.D. Achenbach, A.K. Gautesen, and H. McMaken. *Ray methods for waves in elastic solids: with applications to scattering by cracks*. Pitman advanced publishing program, 1982.
- [15] C.A. Schultz and M.N. Toksöz. Enhanced backscattering of seismic waves from a highly irregular, random interface: P-SV case. *Geophysical Journal International*, 117(3):783–810, 1994.